MET O 11 TECHNICAL NOTE No 203

USING AN INTERACTIVE RADIATION SCHEME IN THE FINE MESH MODEL

by

A DARLINGTON

March 1985

Met O 11 (Forecasting Research)
Meteorological Office
London Road
Bracknell
Berkshire

1. Introduction

An interactive radiation scheme has been developed for use in the operational forecast models from that currently used in the Met O 20 general circulation model. The theory of the scheme is given in the Appendix. As in the Met O 20 scheme, provision is made for two types of cloud: layer and convective. Layer cloud can occur in at most three layers, called high, medium and low, determined by the model's relative humidity field and assumed to be one layer thick. Convective cloud amounts are determined by the convective mass flux, and the top and base of a convective tower are set at the initiating and detraining levels for a convective plume as calculated in the model's deep convection scheme. Water vapour and carbon dioxide are the two absorbing gases treated. For reasons of economy, there is no treatment of ozone and solar radiation is reflected straight to space.

This paper describes the results of some tests recently carried out using the interactive radiation scheme in the operational fine mesh model. As a control, the results are compared with runs using the climatological radiation scheme described by Dickinson and Temperton (1984). The paper concentrates on the impact of the scheme on surface temperature, thickness and precipitation forecasts. Further comments on the frequency of calling of the radiation routines and on the need for a treatment of fog are also included.

The interactive radiation scheme has been operational in the fine mesh model since September 1984, but it has not been possible to include it in the global model until the enhancement of the Cyber 205 memory to 2 Megawards (February 1985). Some further testing of the scheme is necessary before it can be included in operational global forecasts.

The version of the interactive radiation scheme used in the experiments described here includes the modifications to the infra-red calculations devised by Slingo and Wilderspin (1984). Without these changes the scheme can lead to excessive overnight cooling at the surface. This was a feature of many fine-mesh forecasts during the winter of 1984-1985.

2. Cloud cover

A problem that has occurred with the inclusion of an interactive radiation scheme in the Met O 20 general circulation model is the excessive cloudiness of the the maritime boundary layer, especially in the tropics. It was feared that incorporating the same scheme in the fine mesh model might lead to a similar problem. However, in the cases studied for this work, this has not been the case. Many of the tests show an extremely good temperature structure, where cloud has been correctly forecast. Notable amongst these are the forecasts for 06Z on 17/5/84 (T+30) and from DT 00Z 28/5/84.

Figure 1a shows the observations for 0600Z on 17/5/84. Notice the almost clear skies over Ireland, with screen temperatures reported as low as 1°C, indicating a ground frost. Britain, however is overcast with screen temperatures at 7-9°C. Figure 1b gives the surface temperature as predicted by the operational model with the climatological radiation scheme for the same time. It should be borne in mind that at this time a strong surface inversion might be expected, and consequently the model surface temperatures should be lower than the observed screen temperature. Model sigma level 1 temperatures were some 2°C warmer at this time. Temperatures over Ireland lie between 5 and 8°C while over Britain temperatures range over about 9°C in the south to 6°C over the Scottish Highlands. Figure 1c shows the surface temperature as predicted by the operational model with the interactive radiation scheme. The ground frost over Ireland is very well forecast, as are higher surface temperatures over mainland Britain (temperatures generally in the range 6-9°C).

Figures 2a and 2b give the observations for 1200Z on 28/5/84 and 1200Z on 29/5/84. On 28th May much of England and Wales was covered by low stratus cloud, with a typical screen temperature of 10°C. Scotland and Ireland, however, remained relatively clear with temperatures reaching 15°C on the west coast of Scotland and 17°C in central Ireland. 24 hours later the stratus has all but cleared the British Isles, just covering Kent and East-Anglia. The maximum temperature is now recorded near the Bristol Channel.

Figures 2c and 2d are the corresponding forecasts of surface temperatures from the model with climatological radiation. Model predicted surface temperatures will be higher than observed screen temperatures in this case as the overnight surface inversion will have been eroded and replaced by a superadiabat. The T+12 forecast is typical of the climatological scheme which takes no account of cloud variation, in that there is little detail to the temperature structure. Highest temperatures over Britain are forecast in the south east and are some 7°C higher than the observed screen temperature. The forecast for the following day is similar in nature but this time more correct with highest temperatures in the Bristol Channel area.

Figures 2e and 2f are the surface temperature forecasts with interactive radiation included. Temperatures at sigma level 1 are some 3° cooler under clear skies, but similar below clouds. The temperature distribution at T+12 has been captured very well, with temperatures of about 10°C over most of England and Wales and surface temperatures of as much as 18°C over western Scotland and 19°C over Ireland. 24 hours later the temperature field is similar to the operational forecast, with the warmest air in the Bristol Channel area and cooler air in the extreme east and extreme west of the U.K.

At the instigation of the GARP WGNE several different cloud parametrisation schemes have been tested on global forecasts from two data times during the FGGE year (Darlington, 1985). It was hoped that an accurate parametrisation of layer cloud would come from these experiments , but so far no parametrisation scheme has been tried which produces results so much improved on the present simple quadratic in relative humidty as to warrant the extra computational expense. Parametrisations which attempt to use the model's vertical velocity field have suffered from the noise which is evident in this field at upper levels.

3. Rainfall

Several tests have been run on well documented rainfall cases. The main

conclusion from these tests is that the interactive radiation scheme can have the effect of reducing rainfall accumulations through the convective scheme. The clearest cases have occurred in the summer months, when convection appears to have been damped because of an improved forecast of the low level temperature structure. The reduction in winter is not as dramatic although in frontal situations convection is again suppressed with a corresponding reduction in accumulations.

Two examples are presented here. The first (figure 3) demostrates the damping of an isolated storm. Figure 3a shows the observed rainfall accumulations from 6Z on 24/7/84 to 12Z on 24/7/84. Figure 3b gives the corresponding accumulations from a 6-12 hour forecast using the model with climatological radiation, which were mostly convective in nature and figure 3c those from the equivalent run with interactive radiation. It is immediately apparent that the storm over Normandy has been damped in the run with interactive radiation, and that the accumulations forecast by this model are closer to the observed values.

A more striking example is presented in figure 4. In figure 4a we see the observed accumulations for 12-18Z on 17/5/84. Figure 4b gives the 24-30 hour forecast accumulations, and figure 4c the convective contribution to these totals, from the model with climatological radiation. Attention should be centred on two areas: the showers over central England and Wales, which appear to be overdone, and further east, the frontal band curving from Sweden down west of Denmark into Germany. Again, certain grid points receive an excessive amount of convective precipitation. Figure 4d is the corresponding chart from a run with interactive radiation, and once again the convection is seen to be damped. Most impressive is the absence of storms over Sweden and Denmark, and the shift of the main frontal precipitation to northern Germany.

4. Thickness.

(i) 1000 - 950 mb.

An important element of winter forecasting is the ability to predict snow. The operational forecast model uses the 1000 - 850 mb thickness to assign probabilities of precipitation falling as snow. It is therefore important that the forecasting of this variable is not impaired by the introduction of an interactive radiation scheme. The scheme has little effect on the 1000 - 850 mb thickness in the cases studied so far. The case of 16th January 1984 is typical and displayed in figure 5. The verifying thickness chart is shown in figure 5a, a 36 hour forecast using climatological radiation in figure 5b and the forecast with interactive radiation in figure 5c. Whilst it is clear that the model has made a bad timing error in moving the warm air on too fast, the actual differences between the two forecasts are slight.

(ii) 1000 - 500 mb.

Detailed case studies on particularly bad 1000 - 500 mb thickness forecasts have not yet been made. The interactive radiation scheme has made small differences of about 2 dm at most in the cases studied so far. The example shown in figure 6 is again the 36 hour forecast from 0Z on 16/1/84; figure 6a is the verification, 6b the forecast using climatological radiation and 6c the forecast with interactive radiation. The model with interactive radiation is slightly warmer, but again the differences are slight. The regular statistics provided by Met O 2b are necessary to identify systematic trends in the thickness field.

5. Discussion

(i) The interactive radiation scheme has been seen to improve forecasts of temperatures in the lowest layers. Crucial to this ability is a correct forecast

of low cloud:- a poor cloud forecast leads to a poor temperature forecast. It would seem appropriate, therefore, that if and when a forecaster comes to use the fine mesh surface temperature forecast, he should have available the cloud amounts as used by the forecast. Cloud amounts are stored routinely, and I would suggest that charts of at least low cloud would be a useful adjunct to the model surface temperature forecast.

(ii) An improved low level temperature structure is to be expected to improve the model's convection forecast over land, but there may still be deficiencies in the model formulation which are possibly being disguised by the interactive radiation scheme.

(iii) Convective cloud amounts play a crucial role in determining the radiation budget of the tropics, and so before introducing the scheme into the global forecast model the accuracy of the amounts forecast by the convection scheme must be examined.

(iv) The problem of excessive cloudiness in the tropical maritime boundary layer which is apparent by day 4 of a general circulation run must also be investigated before the scheme can be used in the global forecast model.

(v) In operational use of the radiation scheme, a tendency to cool excessively in winter under clear skies has been noticed. This problem has been partially rectified by using the latest scheme used in the climate research branch, but the problem is still there. As an example, figure 7a shows the observations at 06Z on 9th December 1984. Figure 7b shows an 18 hour forecast of surface temperature verifying at this time using the interactive radiation scheme. Notice in particular that the values over Ireland are too cold by approximately 4°C (allowing for a surface inversion). This appears to be due to the formation of fog, which is not modelled at all. A simple way to include the insulating effect of fog is to allow low cloud to occur in the second layer of the model, between σ = 0.997 and 0.975. This is not done at present. A model run with this very simple modification included is shown in figure 7c and it can be seen that the temperatures are much more realistic. I therefore recommend that some effort is directed

towards including the radiative effects of fog before next winter.

(vi) The scheme has been written so that the frequency of calling may readily be changed. Three hours is used operationally, and this appears to be satisfactory: for example, figure 8 shows a surface and sigma level 1 temperature forecast from runs where the radiation scheme is called every hour, every 2 hours and every 3 hours. Little difference can be seen. However, the frequency of calling should be investigated further before operational introduction into the global model.

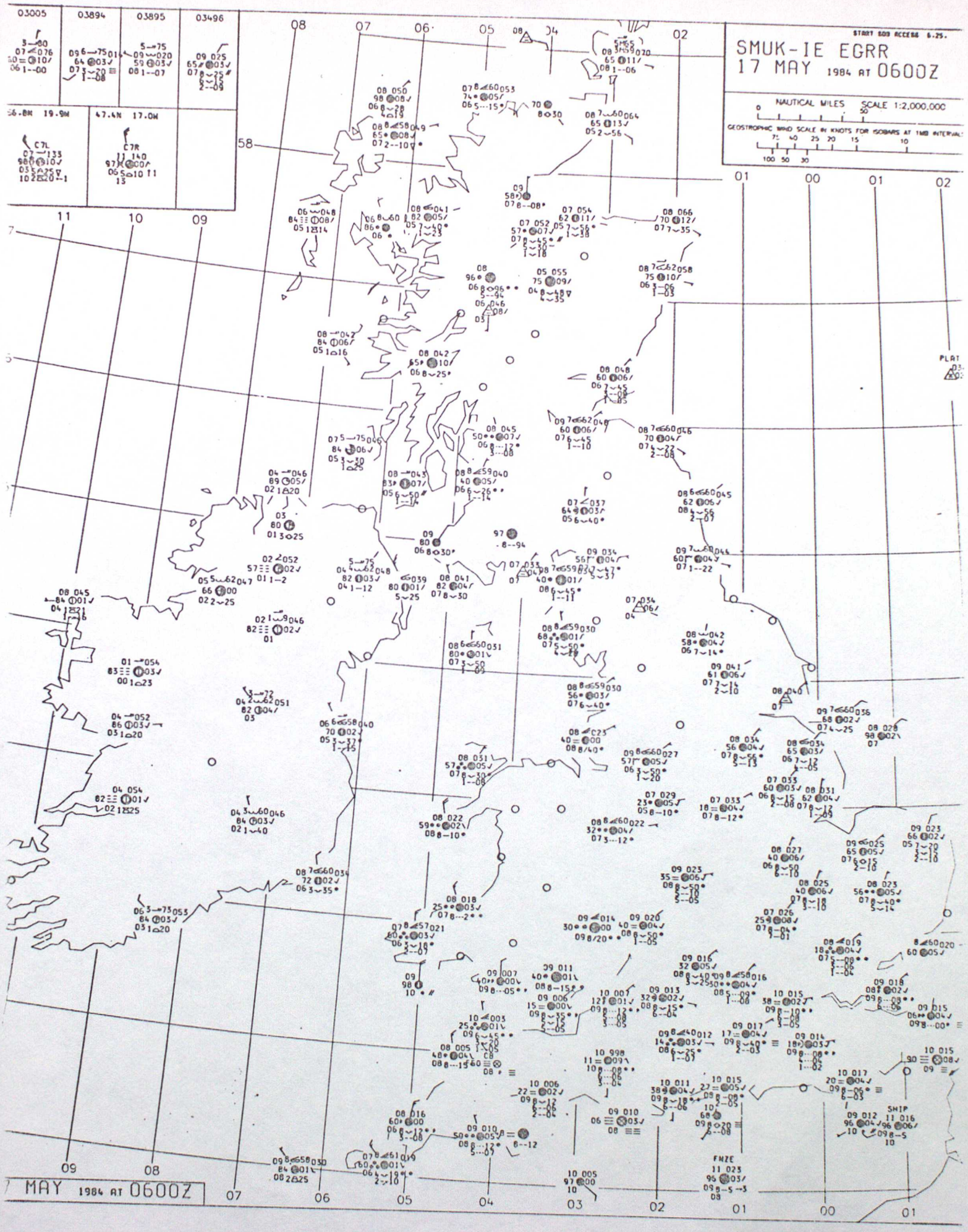
SMUK-IE EGRR
17 MAY 1984 AT 0600Z
NAUTICAL MILES SCALE 1:2,000,000
GEOSTROPHIC WIND SCALE IN KNOTS FOR ISOBARS AT 1MB INTERVAL
MAY 1984 AT 0600Z

Figure 1a

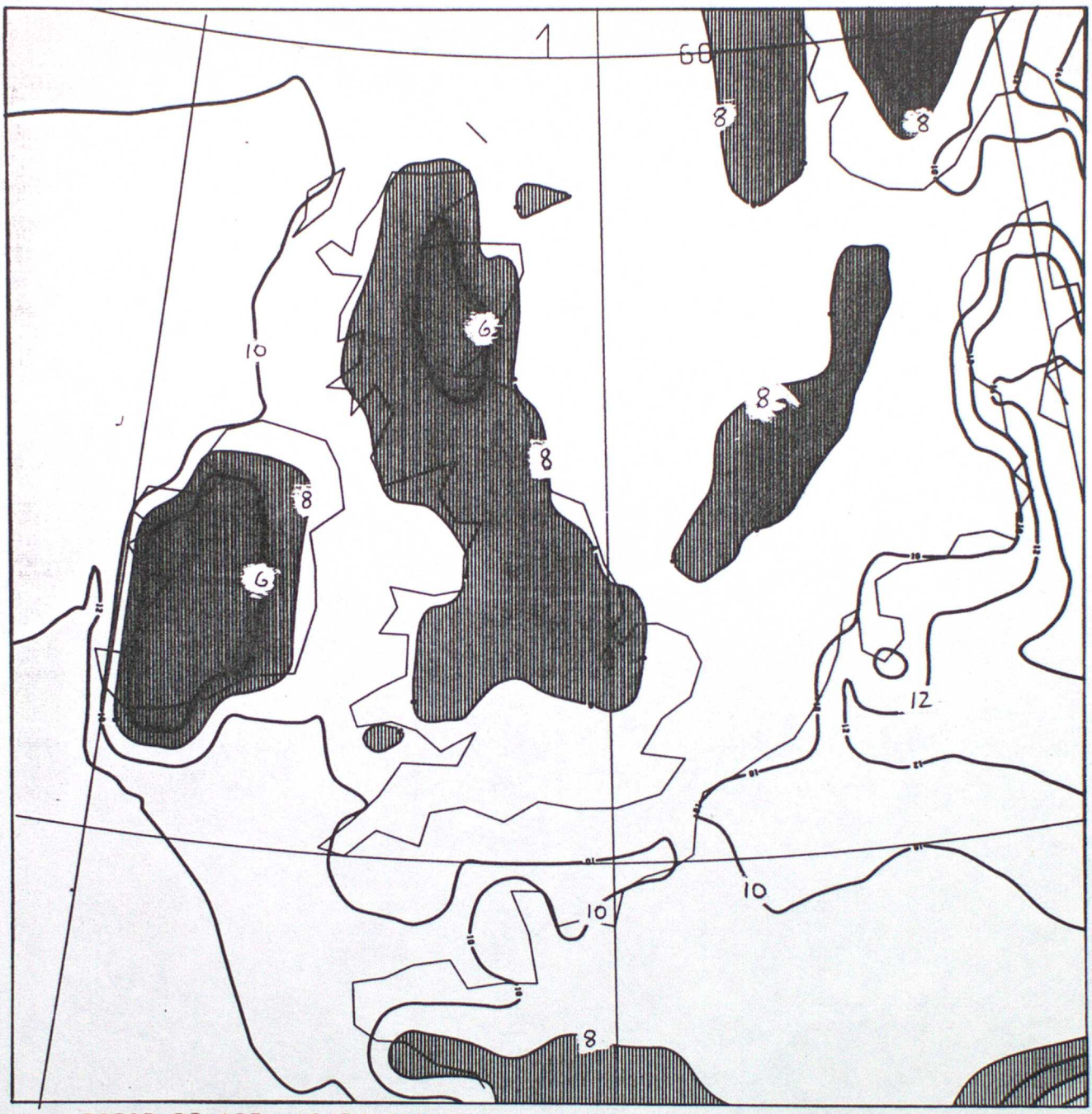

Figure 1b T+18 forecast surface temperatures using climatological radiation.

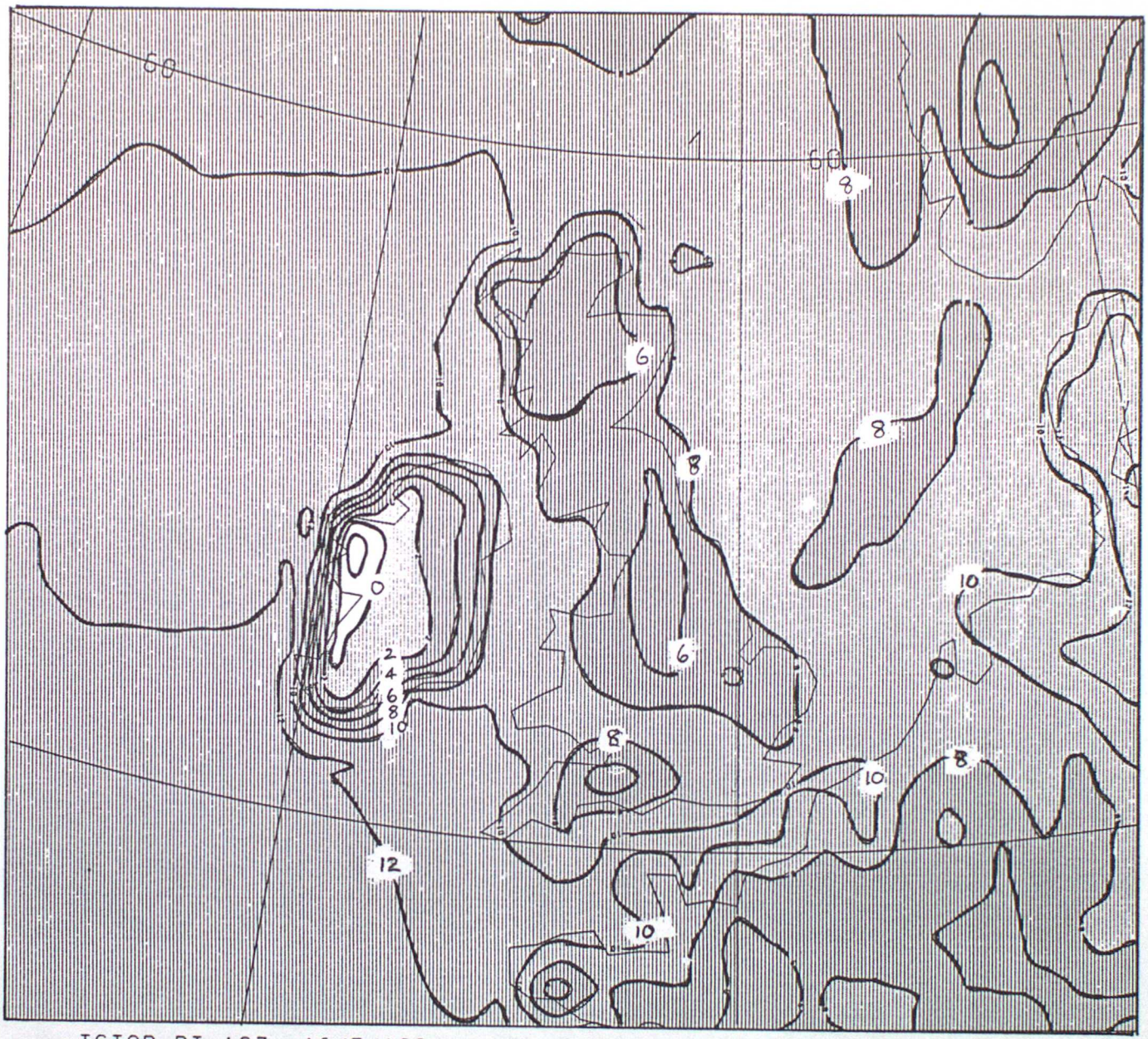

Figure 1c T+18 forecast surface temperatures using interactive radiation.

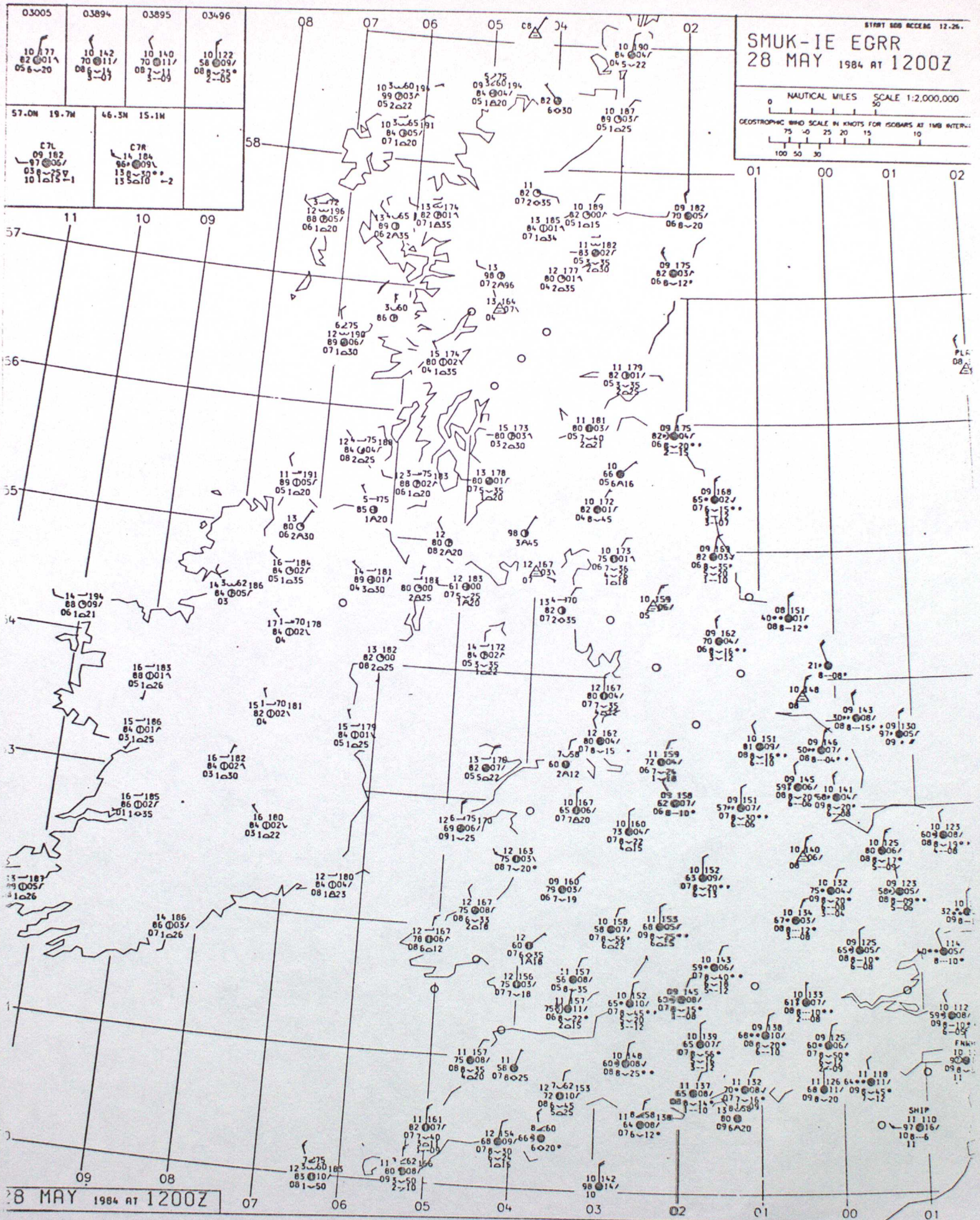
SMUK-IE EGRR
28 MAY 1984 AT 1200Z
NAUTICAL MILES SCALE 1:2,000,000
28 MAY 1984 AT 1200Z

Figure 2a

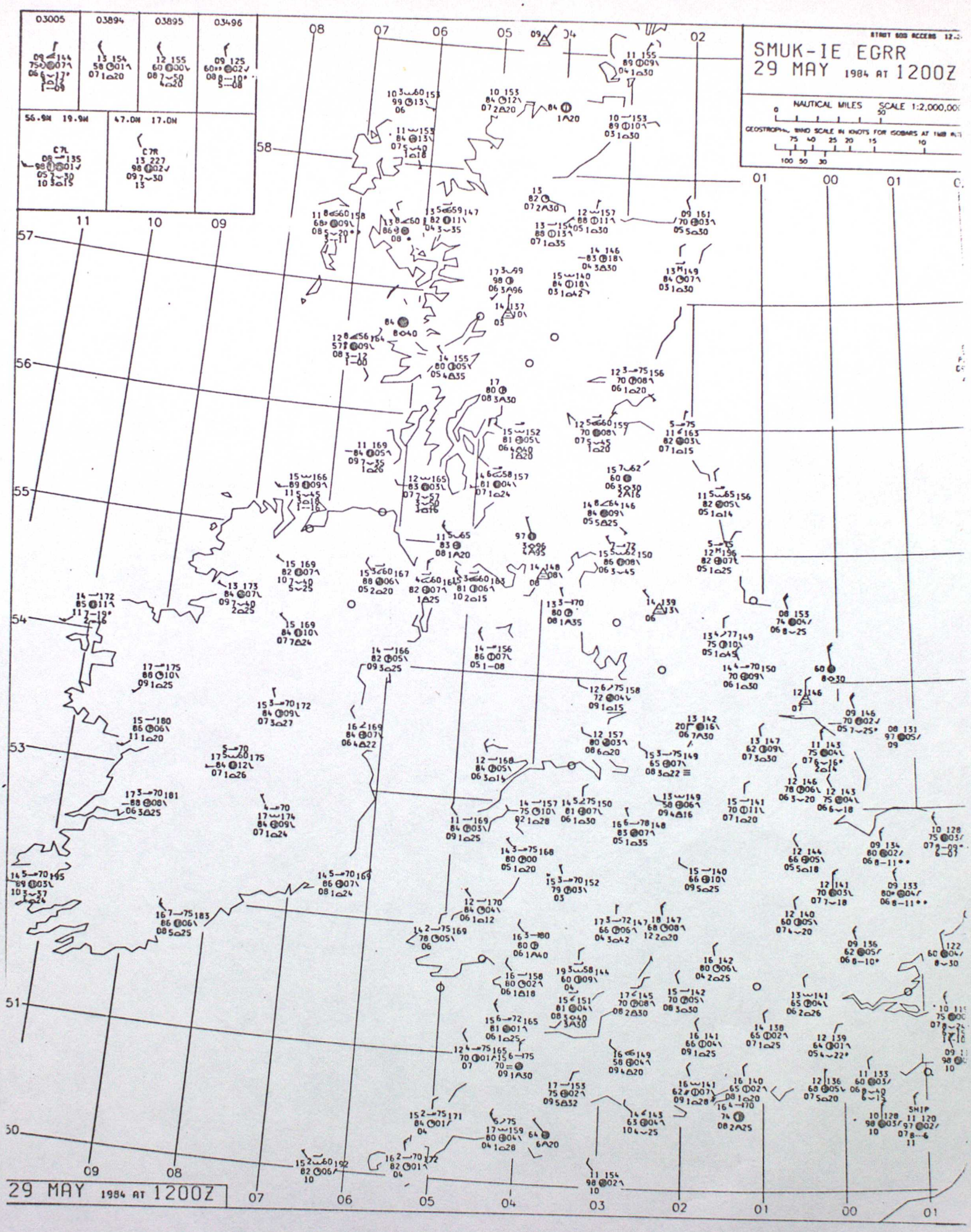
SMUK-IE EGRR
29 MAY 1984 AT 1200Z
NAUTICAL MILES SCALE 1:2,000,000
29 MAY 1984 AT 1200Z

Figure 2b

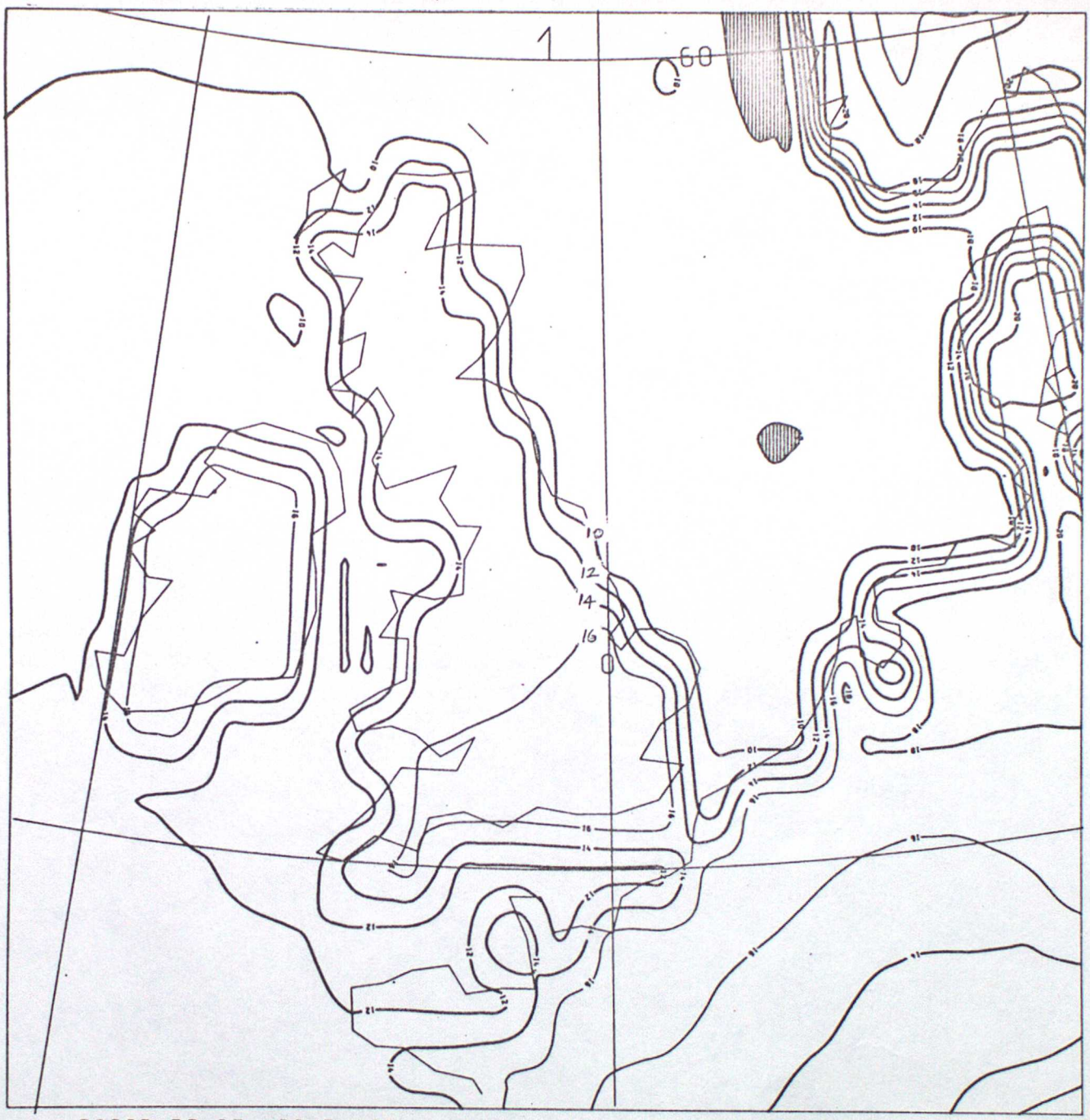

Figure 2c T+12 forecast surface temperatures using climatological radiation.

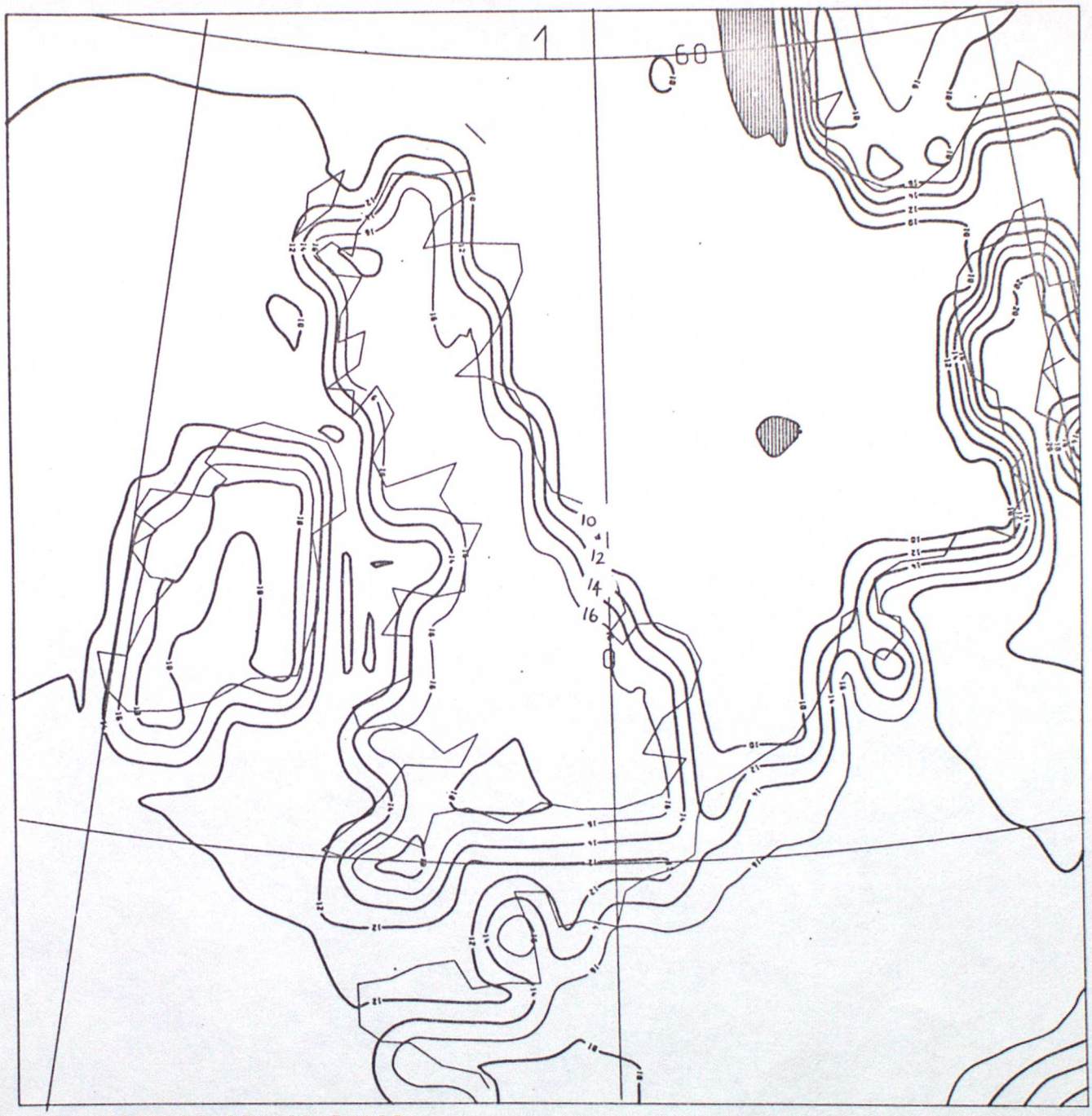

Figure 2d T+36 forecast surface temperatures using climatological radiation.

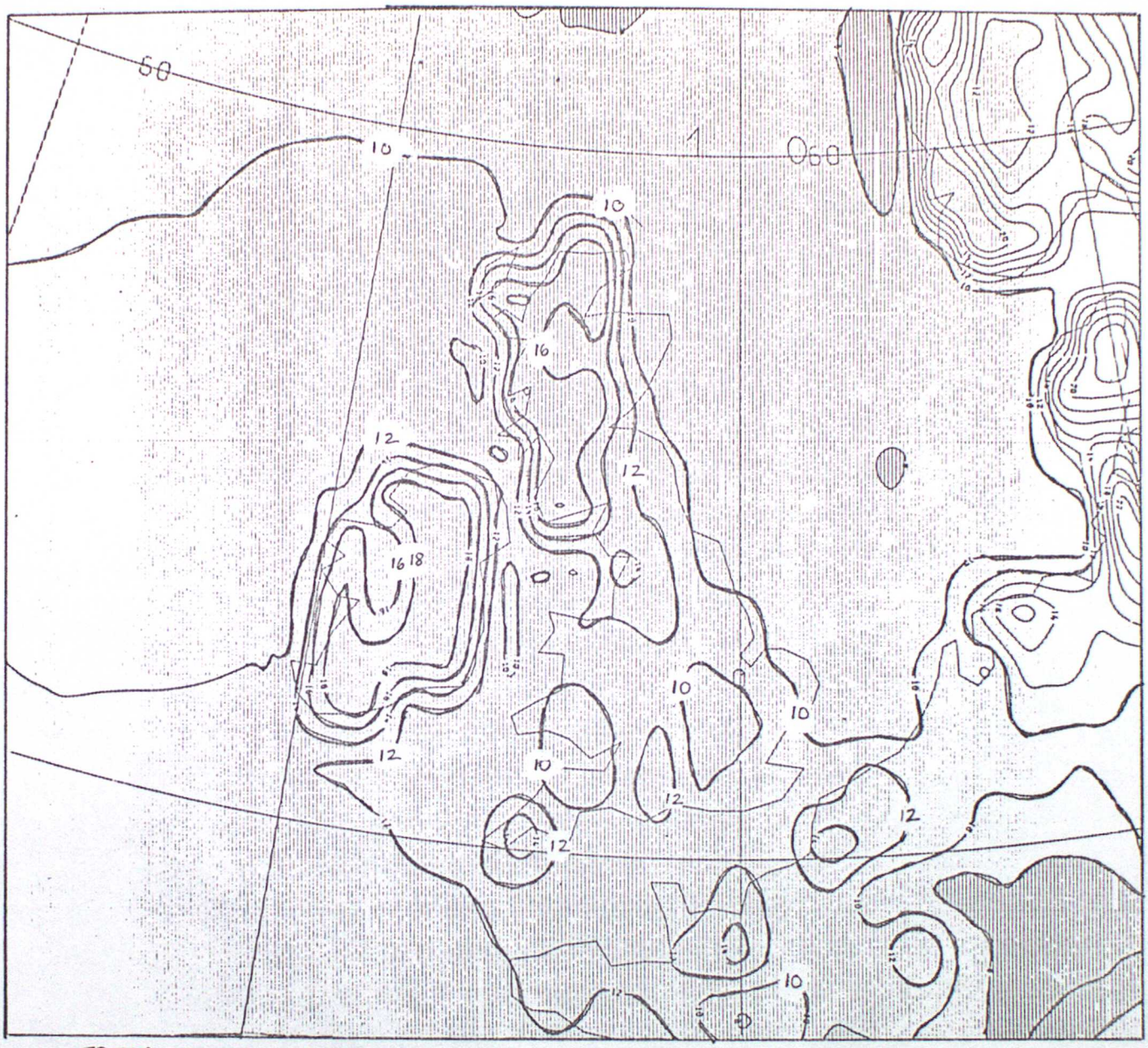

TSTAR DT 0Z 28/5/1984
VT 12Z 28/5/1984

Figure 2e T+12 forecast surface temperatures using interactive radiation.

Figure 2f T+36 forecast surface temperatures using interactive radiation.

6 HOURS OBSERVED ACCUMULATED PRECIPITATION (MM).
FROM 6Z 24/7/84 TO 12Z 24/7/84

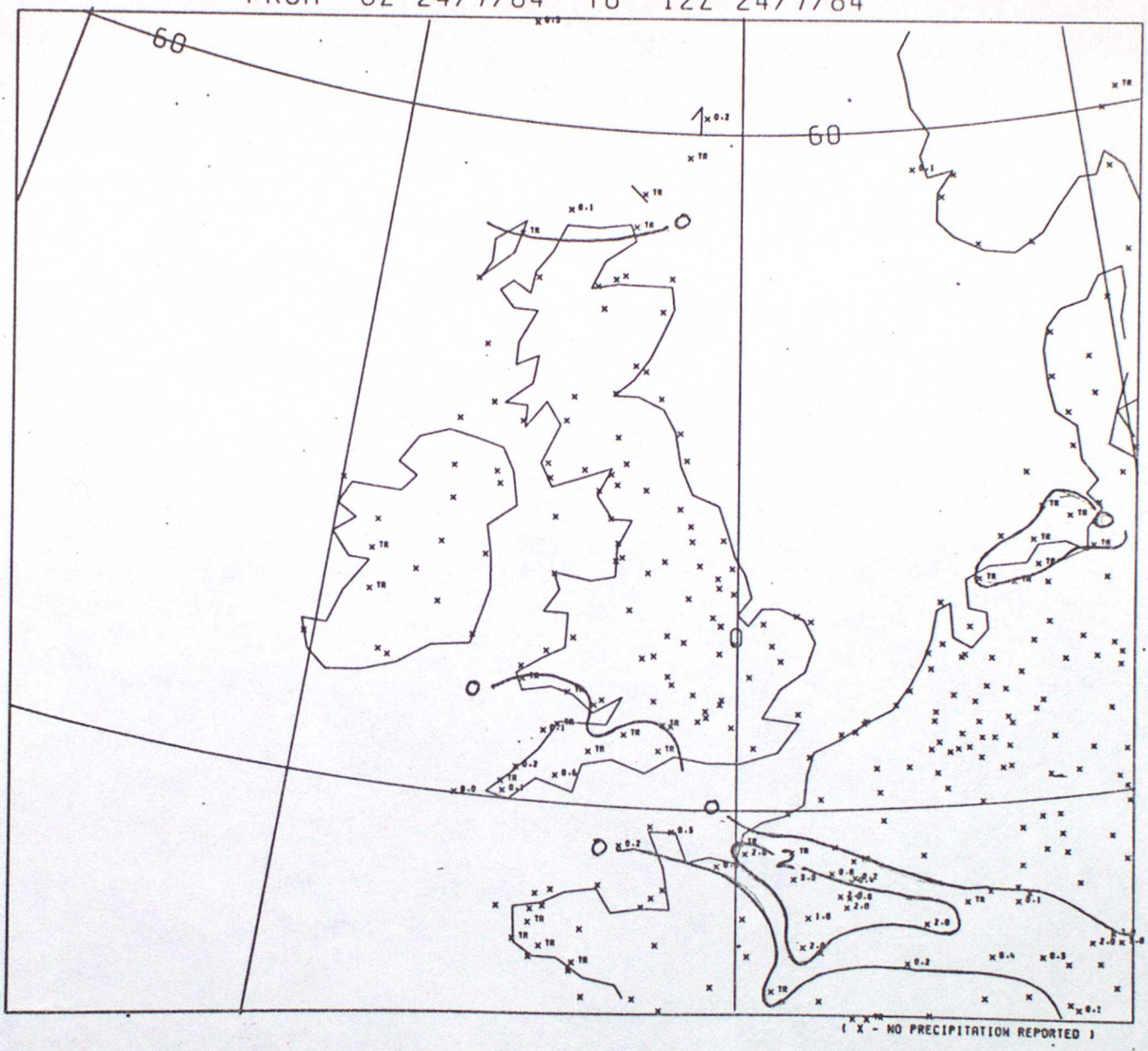

Figure 3a

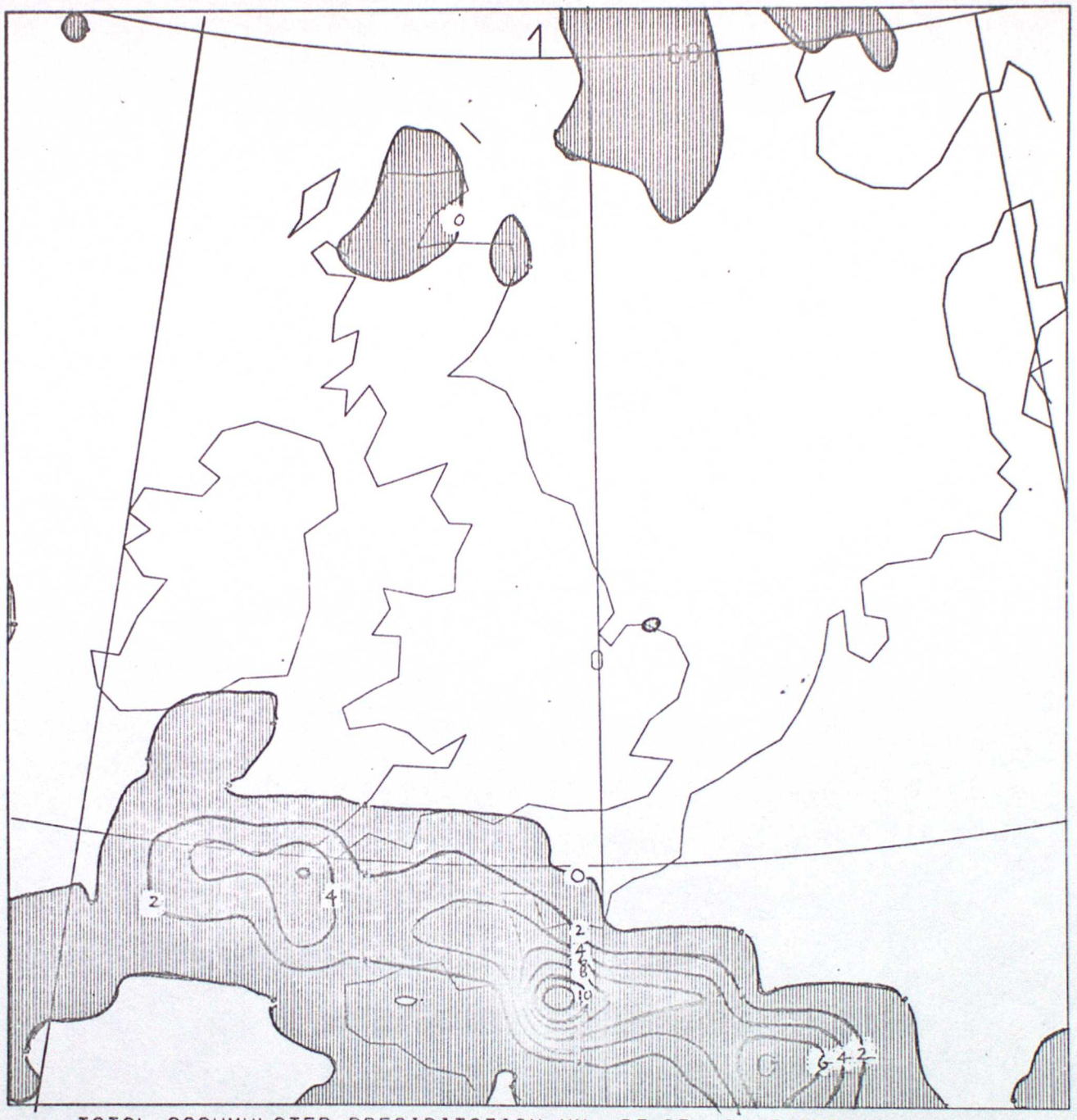

Figure 3b T+6 - T+12 accumulated precipitation using climatological radiation.

Figure 3c T+6 - T+12 accumulated precipitation using interactive radiation.

6 HOURS OBSERVED ACCUMULATED PRECIPITATION (MM).
FROM 12Z 17/5/84 TO 18Z 17/5/84

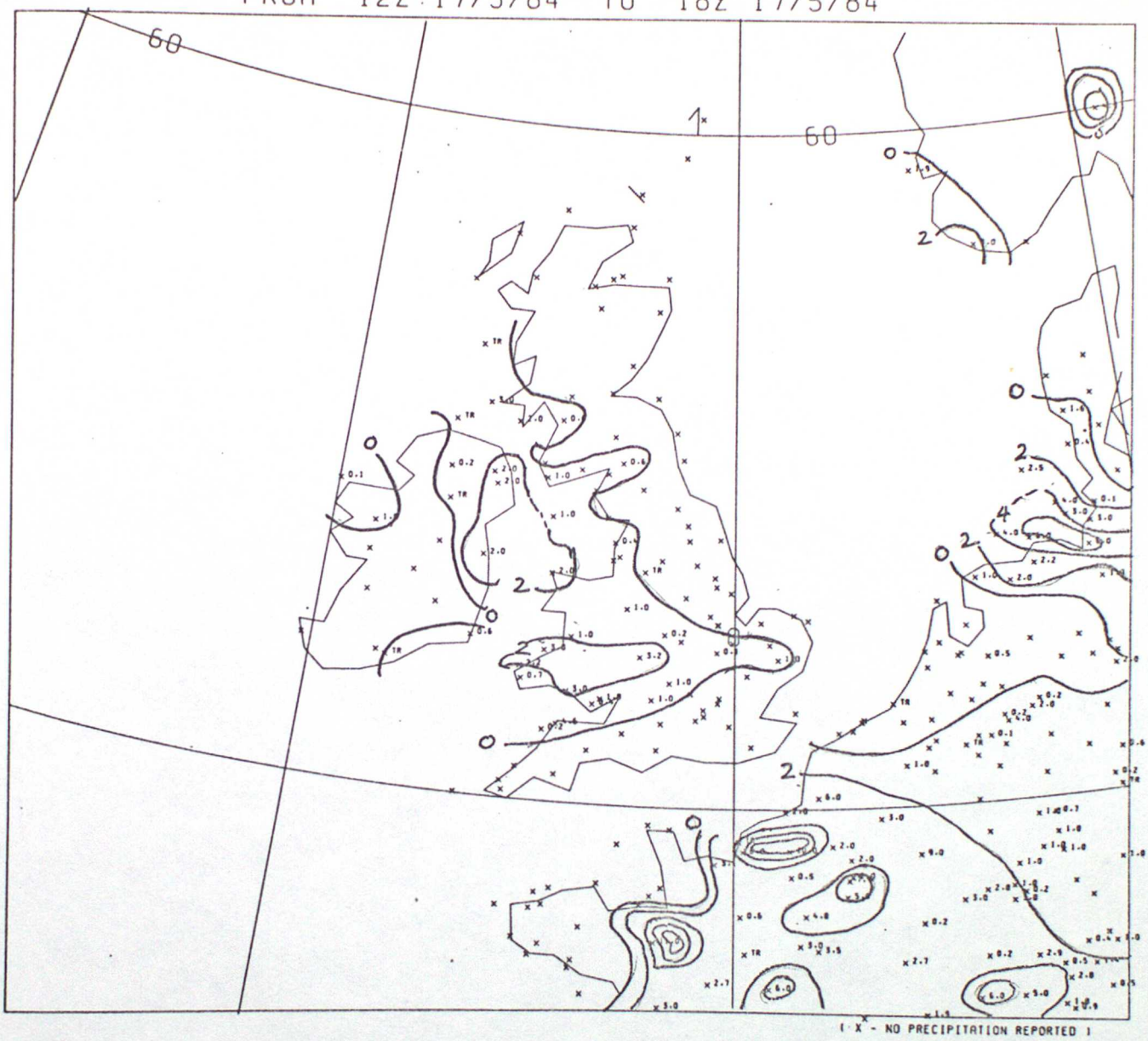

Figure 4a

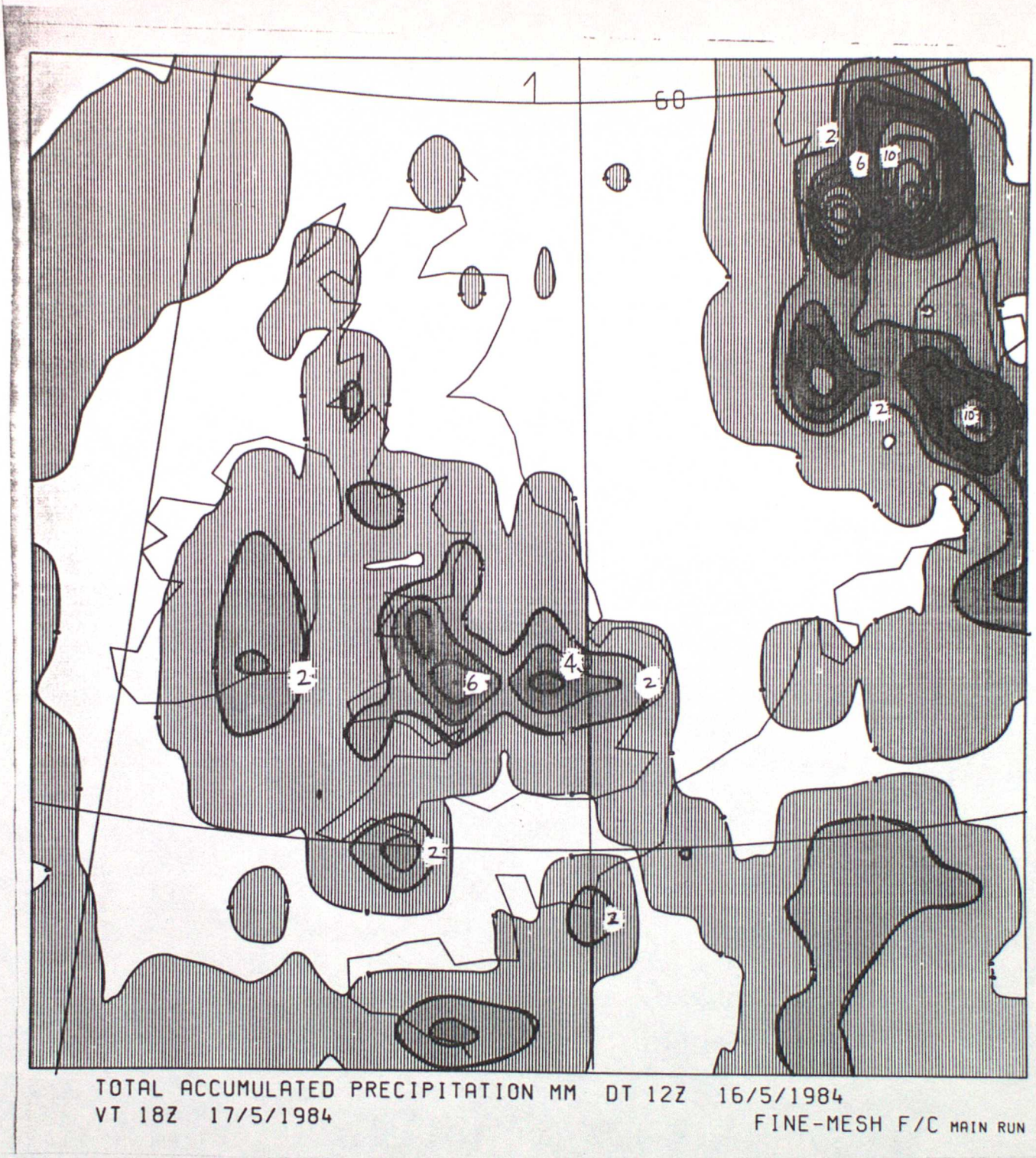

Figure 4b T+24 - T+30 accumulated precipitation using climatological radiation.

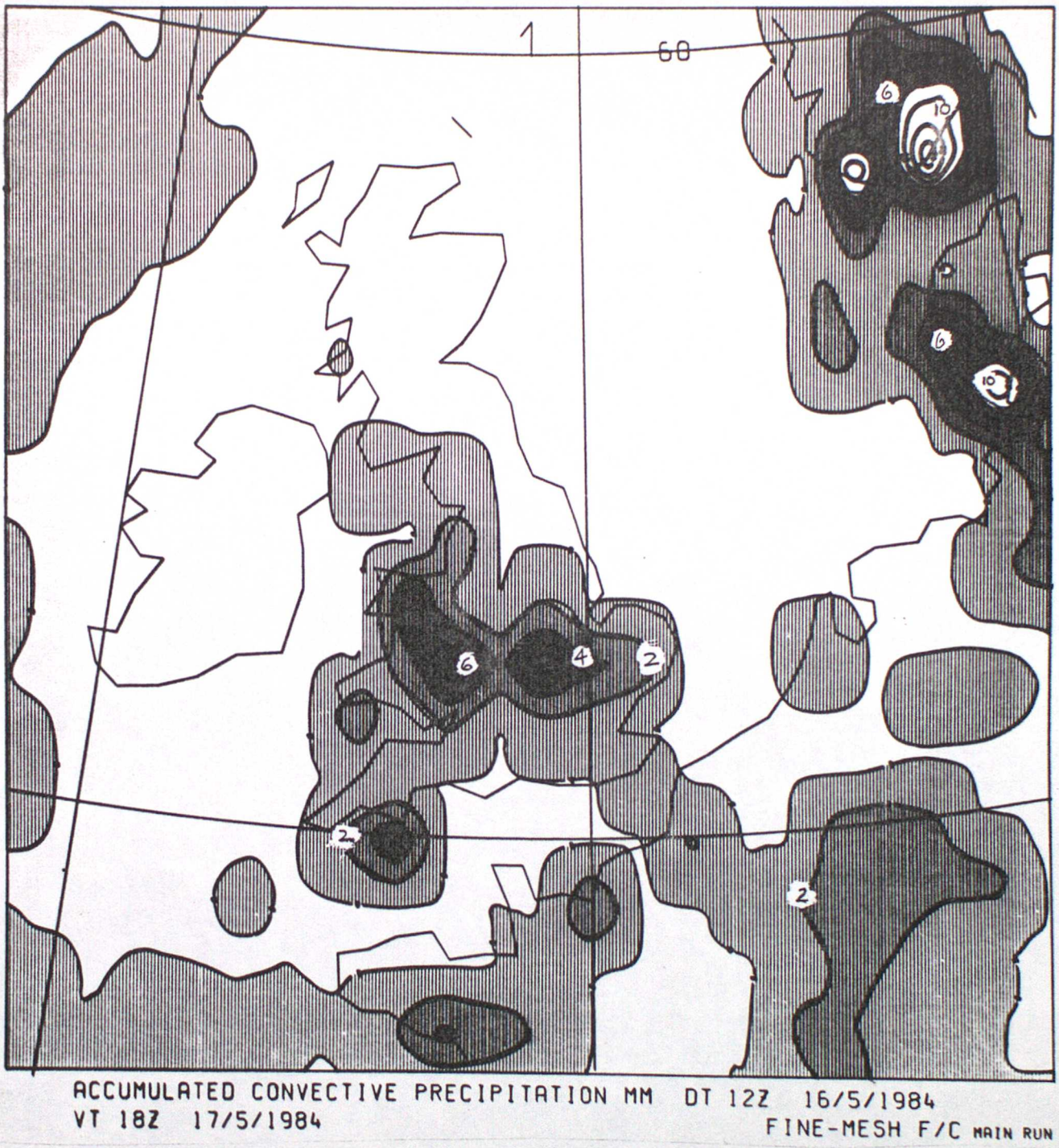

Figure 4c T+24 - T+30 accumulated convective precipitation using climatological radiation.

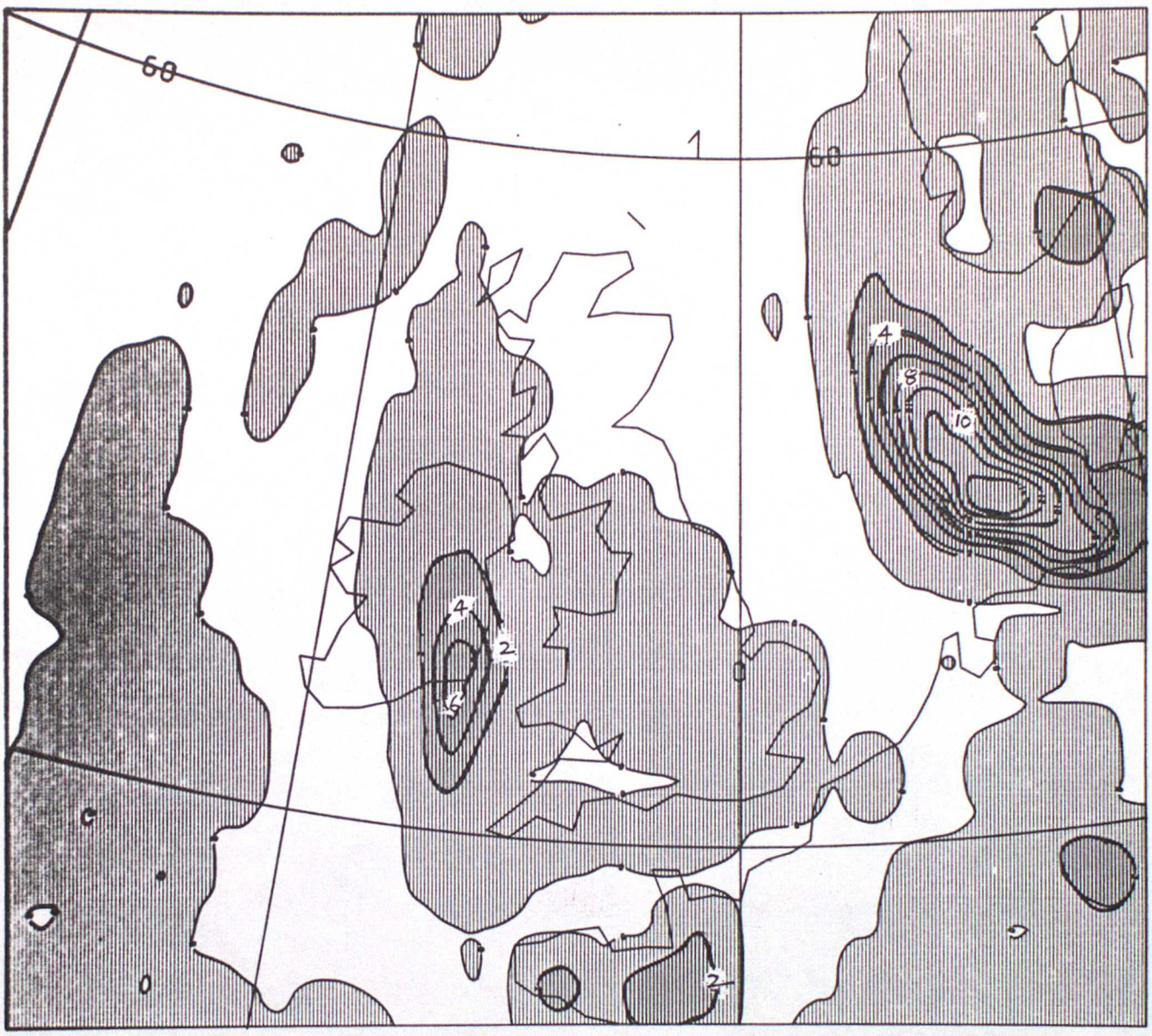

TOTAL ACCUMULATED PRECIPITATION MM DT 12Z 16/5/1984
VT 18Z 17/5/1984 FINE-MESH F/C MAIN RUN

Figure 4d T+24 - T+30 accumulated precipitation using interactive radiation.

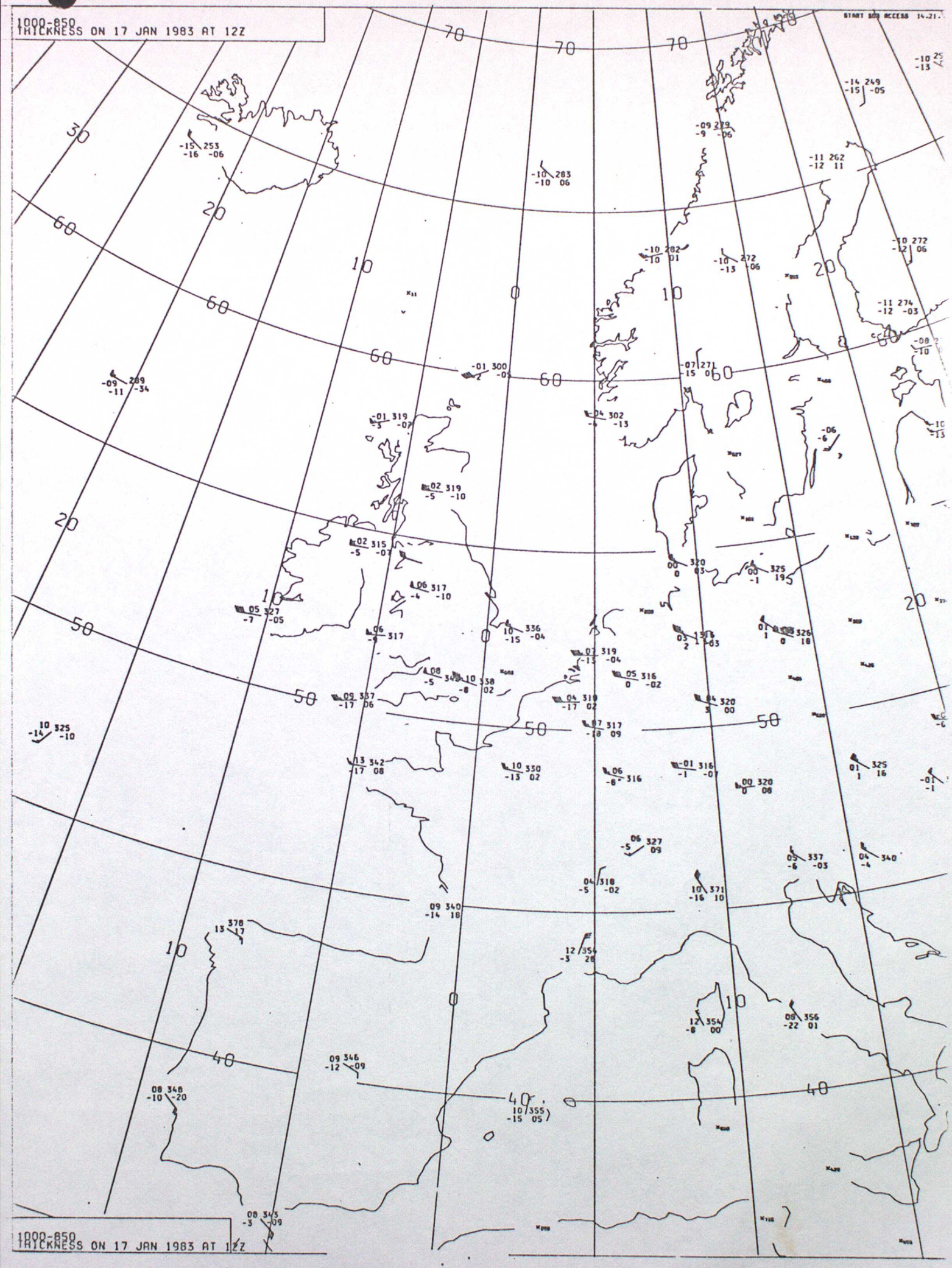
1000-850
THICKNESS ON 17 JAN 1983 AT 12Z
1000-850
THICKNESS ON 17 JAN 1983 AT 12Z

Figure 5a

Figure 5b T+36 forecast using climatological radiation.

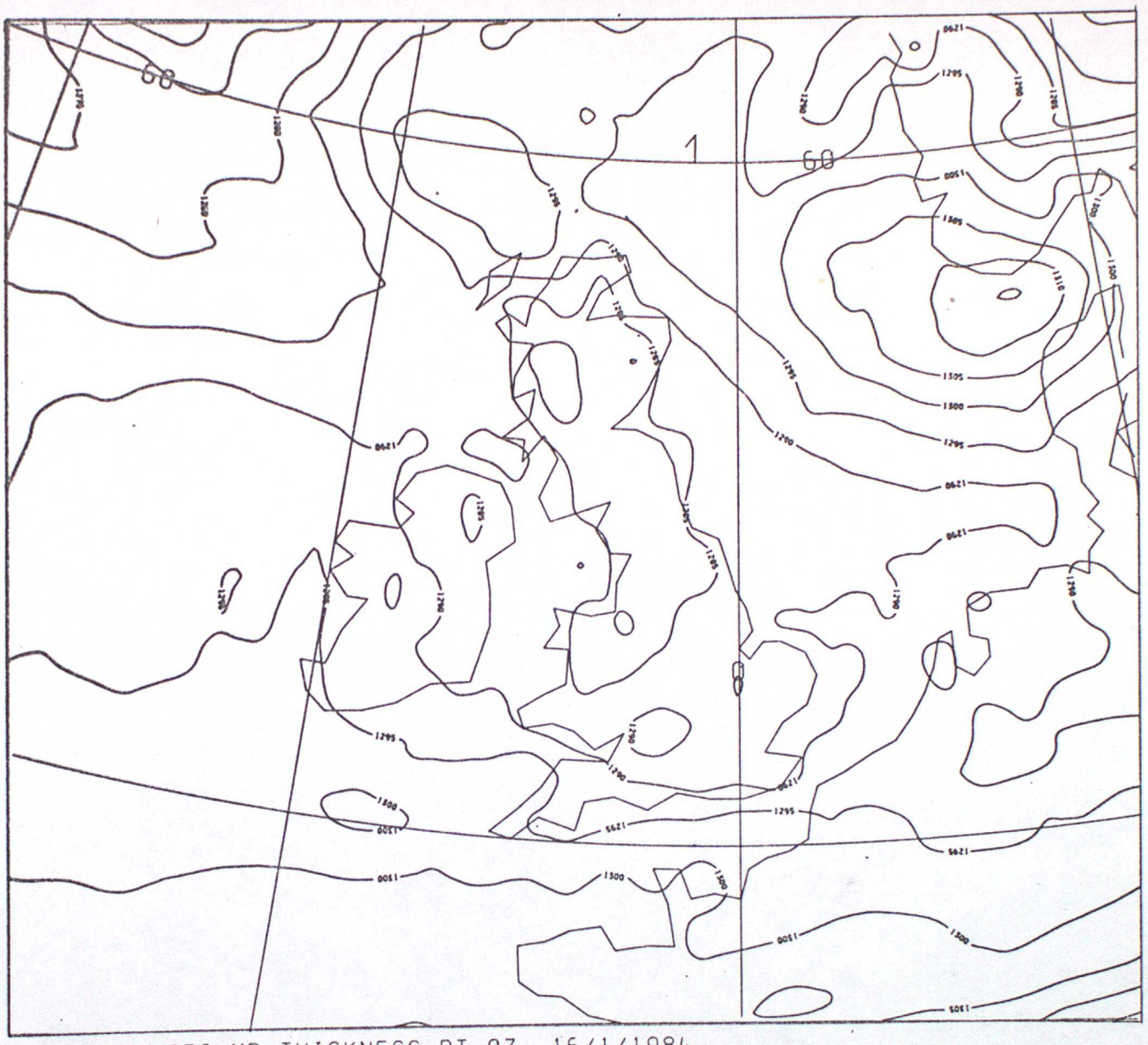

Figure 5c T+36 forecast using interactive radiation.

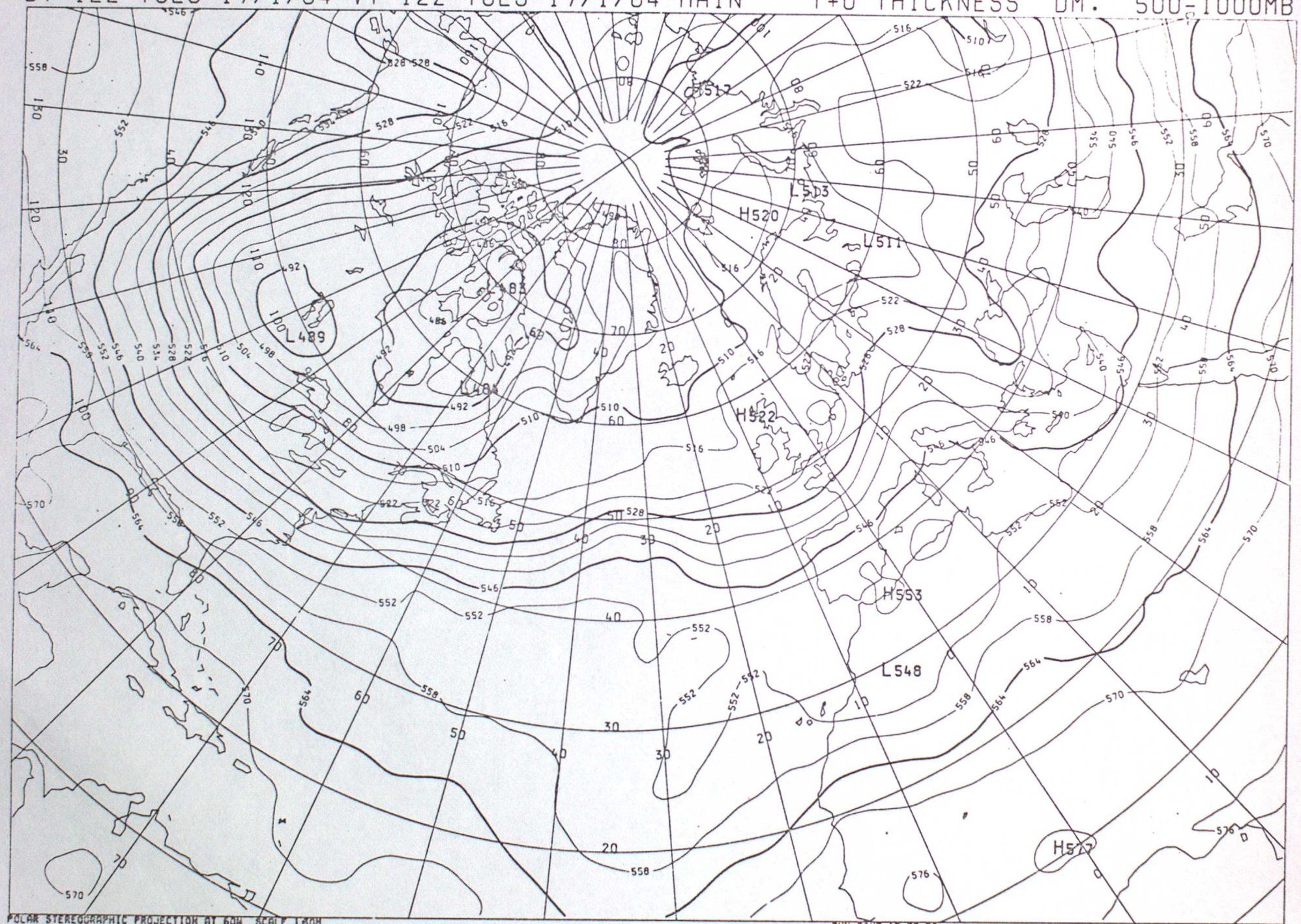
DT 12Z TUES 17/1/84 VT 12Z TUES 17/1/84 MAIN T+0 THICKNESS DM. 500-1000MB
H520
L511
L503
L512
L489
L484
H522
H553
L548
H577
POLAR STEREOGRAPHIC PROJECTION AT 60W SCALE 1:80M
RUN TIME 15.53.50
COP
CHART15

Figure 6a

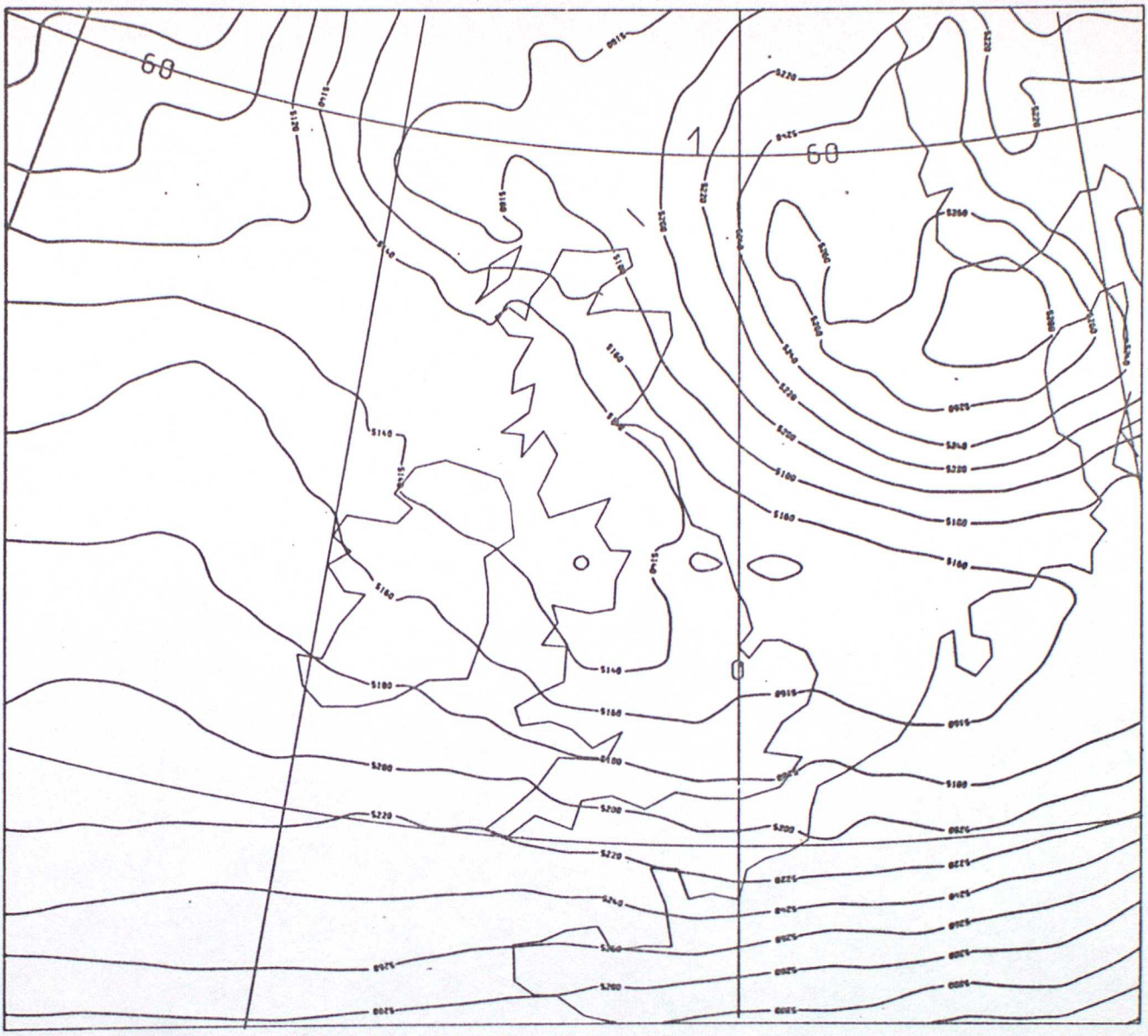

Figure 6b T+36 forecast using climatological radiation.

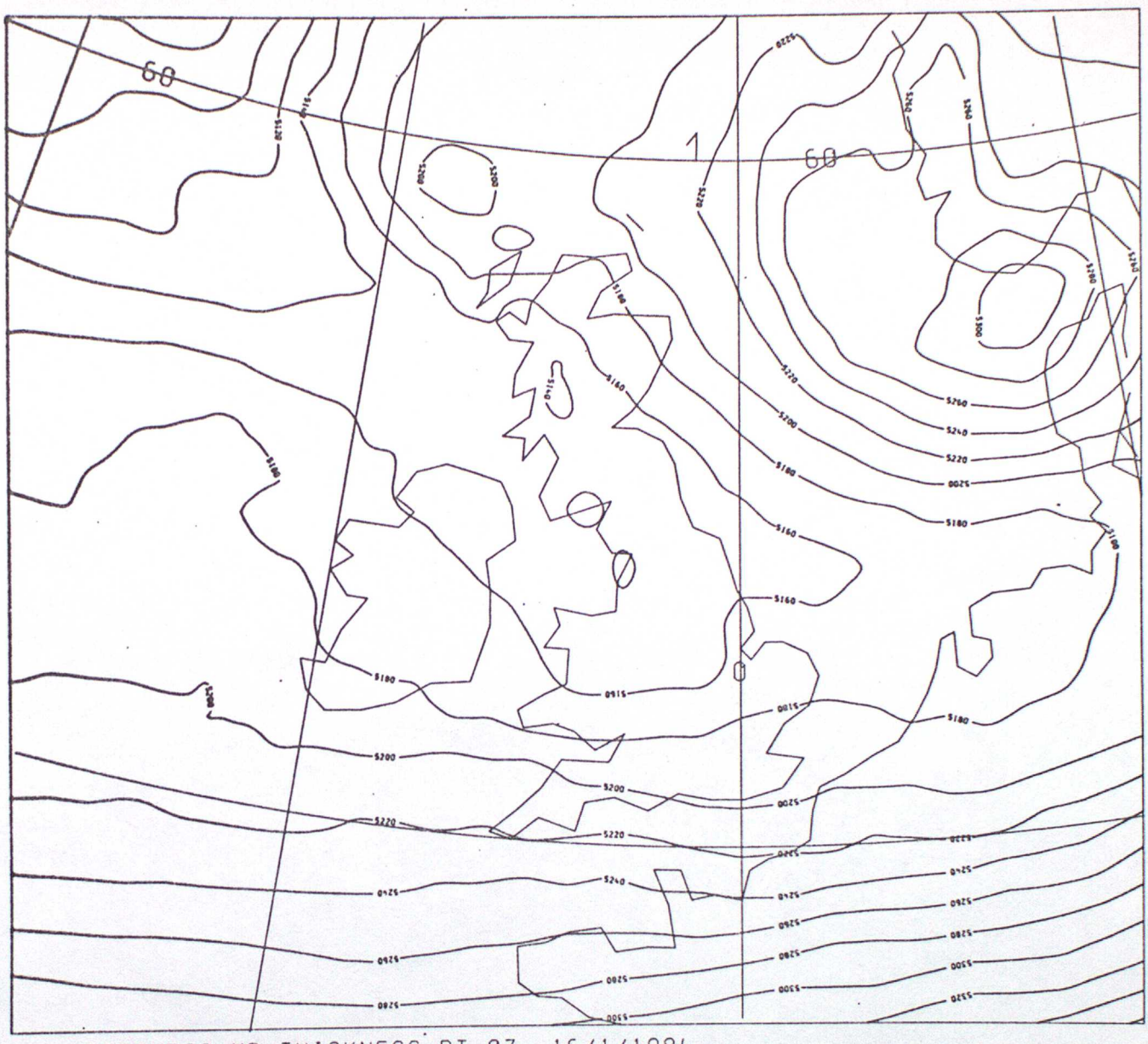

Figure 6c T+36 forecast using interactive radiation.

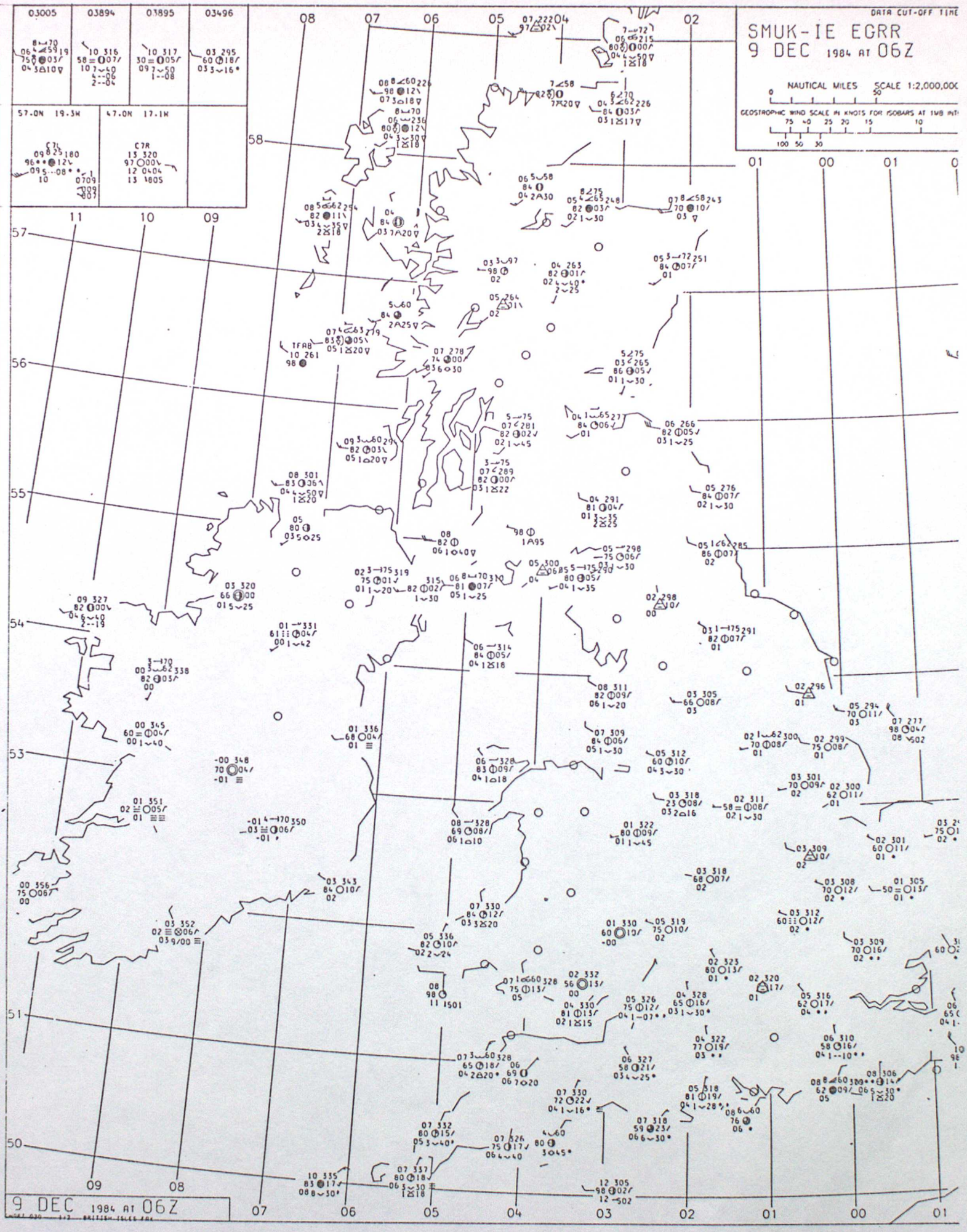
SMUK-IE EGRR
9 DEC 1984 AT 06Z
DATA CUT-OFF TIME
NAUTICAL MILES SCALE 1:2,000,000
GEOSTROPHIC WIND SCALE IN KNOTS FOR ISOBARS AT 1MB INTERVALS
03005
03894
03895
03496
57.0N 19.3W
47.0N 17.1W
9 DEC 1984 AT 06Z

Figure 7a

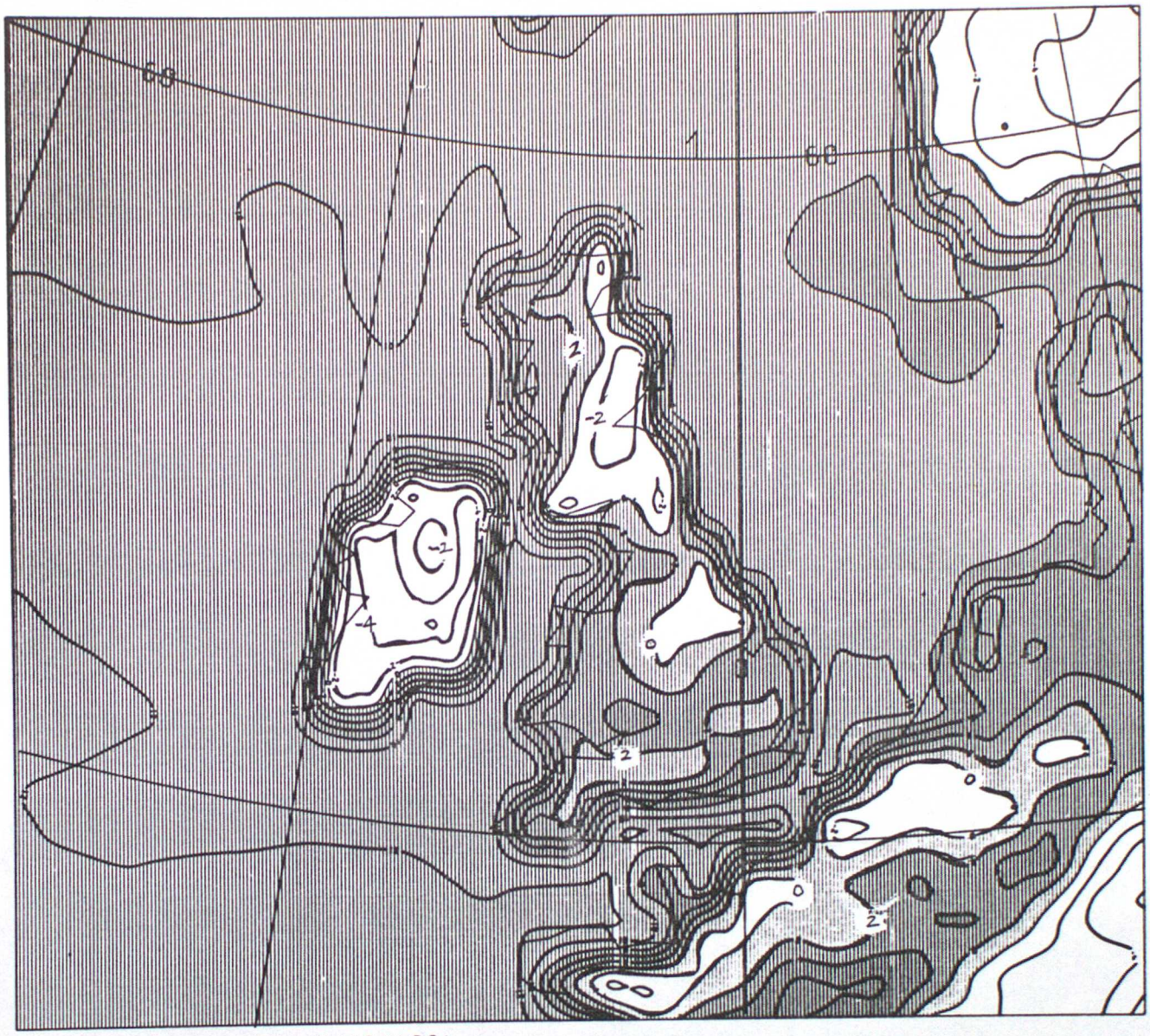

Figure 7b T+18 forecast surface temperatures using interactive radiation.

Figure 7c T+18 forecast surface temperatures using interactive radiation with layer cloud allowed to form in the bottomost model layer.

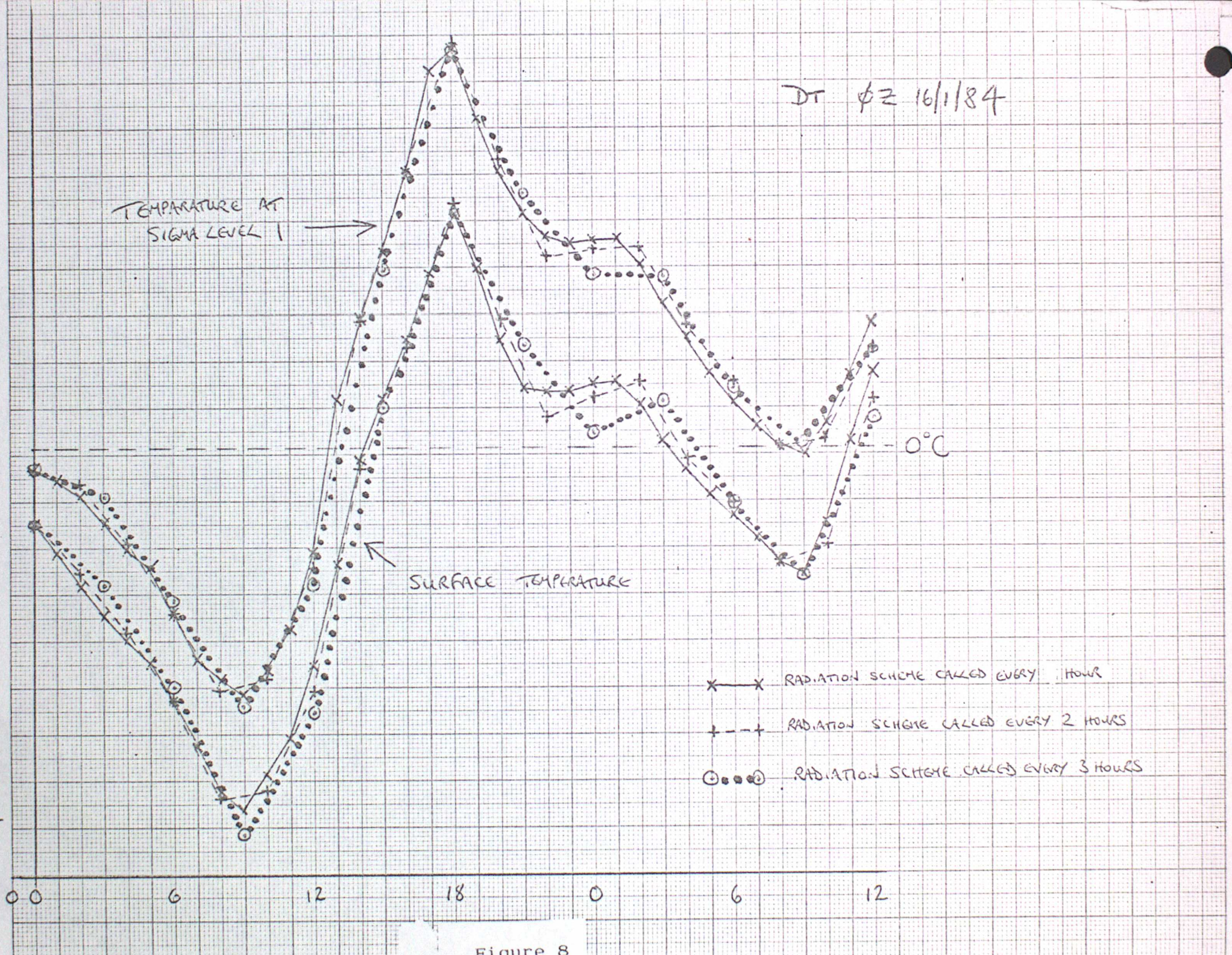
DT ϕZ 16/1/84
TEMPARATURE AT SIGMA LEVEL 1
SURFACE TEMPHRATURE
0°C
RADIATION SCHEME CALLED EVERY 1 HOUR
RADIATION SCHEME CALLED EVERY 2 HOURS
RADIATION SCHEME CALLED EVERY 3 HOURS
282
281
280
279
278
277
276
275
274
273
272
271
270
269
268
267
266
265
264
0 0
6
12
18
0
6
12

Figure 8

9 INTERACTIVE RADIATION

The interactive radiation scheme is based on the experience of many in the dynamical climatology branch, most recently Slingo and Wilderspin (1984). Flux differencing is used to obtain heating rates at the surface and at all layers of the model atmosphere. A full calculation of radiative fluxes is performed at regular intervals during the model integration with the radiative cooling and heating effects being meaned over the time until the next radiation calculation. The time between full radiation calculations is currently three hours, and the radiative heating rates are held constant during this time.

Two actively absorbing gases are treated by the scheme: water vapour and carbon dioxide. The specific humidity of the model is assumed to describe the water vapour distribution and both the band absorption and the water vapour continuum are treated. Carbon dioxide is assumed well mixed throughout the atmosphere with a mixing ratio of 4.9×10^{-4} kg kg^{-1}.

Four cloud types are catered for in the scheme: high, medium and low layer cloud, and a convective tower. Random overlap of clouds is assumed, and the cloud optical properties are fixed.

As in the climatological scheme, we divide the flux calculations into solar and longwave radiation.

9.1 The flux of longwave radiation

In the development of the theory we assume that there is only one cloud layer. The extension to several randomly overlapped cloud layers is trivial. The total downward radiative flux at height z will, in general, have two components - the clear sky downward flux and the downward flux from the cloud base: thus

$$I\ (z) = (1-Q)\ I^{\infty}\ (z) + QI^{C}\ (z) \tag{9.1}$$

where Q is the cloud amount and $I^{\infty}(z)$ is the clear sky flux, given by

$$I^{\infty}(z) = \int_{o}^{\infty}\{\pi B_{\omega}(T_z) - \pi B_{\omega}(T_{\infty})\gamma_{i\omega}(z,\infty)\}d\omega - \int_{o}^{\infty}d\omega\int_{T_z}^{T_{\infty}}\pi\gamma_{i\omega}(z,z')\frac{dB_{\omega}(T_{z'})}{dT_{z'}}\,dT_{z'} \tag{9.2}$$

Here $\gamma_{i\omega}$ is the flux transmittance or transmission function for gas i, $B_{\omega}(T)$ is the Planck function at frequency ω and temperature T, and T_{∞} is the temperature at the top of the atmosphere.

The flux transmittance is given by

$$\gamma_{i\omega}(z,z') = 2\int_{o}^{\pi/2} e^{-\left[\int_{o}^{yi(z,z')} x_{i\omega}\,\sec\Xi\,dY\right]}\sin\Xi\cos\Xi\,d\Xi \tag{9.3}$$

where $x_{i\omega}$ is the extinction coefficient at frequency ω for gas i and the optical path length, $y_i(z,z')$ is given by

$$y_i(z,z') = \int_o^{z'} \rho_i(\zeta)\, d\zeta - \int_o^{z} \rho_i(\zeta)\, d\zeta = Y(z')-Y(z) \qquad (9.4)$$

where $\rho_i(\zeta)$ is the density of gas i at height ζ.

$I^C(z)$ is the downward flux from the cloud base. All clouds are assumed to be black bodies, apart from high cloud which is assumed to be "grey". This is effected by multiplying the high cloud amount by 0.75, and then treating it as a black body.

$$I^C(z) = \int_o^{\infty} d\omega\ \pi\ B_\omega(T_{cb}) - \pi \int_o^{\infty} d\omega \int_{T_z}^{T_{cb}} \pi\gamma_{i\omega}(z,z') \frac{dB_\omega(T_{z'})}{dT_{z'}}\, dT_{z'} \qquad (9.5)$$

T_{cb} is the temperature at cloud base.

To perform the spectral integration in (9.2) and (9.5) we make use of the emissivity approximation. The spectrum is split into bands over which the emmisivity and absorptivity are assumed to have no frequency dependence. We define <u>partial emissivity</u> as

$$\epsilon_i(\omega_1,\omega_2;z,z') = \frac{\int_{w_1}^{\omega_2} B_\omega(1-\gamma_{i\omega}(z,z'))d\omega}{\int_{\omega_1}^{\omega_2} B_\omega\, d\omega} \qquad (9.6)$$

and <u>partial absorptivity</u> as

$$\tilde{\epsilon}_i(\omega_1,\omega_2;z,z') = \frac{\int_{\omega_1}^{\omega_2} \frac{dB_\omega}{dT}\ (1-\gamma_{i\omega}(z,z'))d\omega}{\int_{\omega_1}^{\omega_2} \frac{dB_\omega}{dT}\ d\omega} \qquad (9.7)$$

On writing $\int_{\omega_1}^{\omega_2} B_\omega(T)d\omega = b_{12}(T)$ (9.8)

equations (10.2) and (10.5) become

$$I^{\infty}(z) = \sum_{\text{Bands}} \left[\pi\, \epsilon_i(\omega_1,\omega_2;z,\infty) b_{12}(T_\infty) - \pi \int_{b_{12}(T_z)}^{b_{12}(T_\infty)} \tilde{\epsilon}_i(\omega_1,\omega_2;z,z')db_{12}(T_{z'}) \right] \quad (9.9)$$

and

$$I^{C}(z) = \sum_{\text{Bands}} \left[\pi\ b_{12}(T_{cb}) - \int_{b_{12}(T_z)}^{b_{12}(T_{cb})} \pi\ \tilde{\epsilon}_i(\omega_1,\omega_2;z,z')d\, b_{12}(T_{z'}) \right] \quad (9.10)$$

Note that the first term here is $\pi\int_o^\infty d\omega B_\omega(T_{cb}) = CT_{cb}^4$, where C is Stephan's constant.

In fact, the absorption spectra of the gases overlap, and so it is not possible to split the spectrum into bands for which just one gas is active. An approximate partial absorptivity and emissivity for the overlap are calculated from the absorptivities and emissivities for the individual gases. We set:

$$\tilde{\epsilon}_{12} \approx 1-(1-\tilde{\epsilon}_1)(1-\tilde{\epsilon}_2) \quad (9.11)$$

$$\epsilon_{12} \approx \epsilon_1 + \epsilon_2 - \epsilon_1\epsilon_2 \quad (9.12)$$

(9.11) is written in this manner because the absorptivity is actually calculated from a table of transmissivities, defined by

$$\tilde{\tau} = (1-\tilde{\epsilon}) \quad (9.13)$$

The bands used in the operational scheme are shown in figure 9.1 (ozone is not included in the scheme, but facility exists for its inclusion).

The water vapour emissivities for the six bands are shown as a function of optical depth in figures 9.2a-f and the transmissivities in figures 9.3a-f. The carbon dioxide emissivity is shown in figure 9.4 and the transmissivity in figure 9.5.

The Planck function integral (9.8) is approximated by a cubic in temperature for each of the six bands.

As in (9.1) the total upward radiative flux at height z will, in general, have two components - the clear sky upward flux and the upward flux from the cloud top: thus

$$I^{\uparrow}(z) = (1 - Q)\, I^{*\uparrow}(z) + Q\, I^{C\uparrow}(z) \qquad (9.14)$$

where $I^{*\uparrow}(z)$ is the upward flux from the surface of the earth,

$$I^{*\uparrow}(z) = CT_*^4 + \sum_{\text{bands}} \int_{b_{12}(T_*)}^{b_{12}(T_z)} \pi\, \tilde{\epsilon}_i\, (\omega_1, \omega_2; z', z)\, db_{12}(T_{z'}) \qquad (9.15)$$

and $I^{C\uparrow}(z)$ the upward flux from the cloud top, which is given by an equation identical to (9.15) but with T_{ct} (the cloud top temperature) replacing T_*.

The extinction coefficient $x_{i\omega}$ seen in (9.3) is known to vary with pressure, which varies along an atmospheric path. This effect can be parametrised by using a pressure weighting of the path length to give an effective optical depth:

$$\bar{y}_i\,(z,z') = \int_{Y(z)}^{Y(z')} \left(\frac{p}{p_o}\right)^{w_i} dY \qquad (9.16)$$

where p is the pressure, p_o is standard atmospheric pressure, (1013.25 mb), w_i is the pressure scaling factor for gas i and Y is as defined in (9.4). Assuming that the mixing ratio q_i of the gas is constant in a layer (σ_1,σ_2) and that we may neglect the term

$$\left(\frac{p*}{p_o}\right)^{w_i} \qquad (9.17)$$

we approximate (10.16) by

$$\bar{y}_i\,(\sigma_2,\sigma_1) \approx q_i\, p* \quad \frac{(\sigma_1(1+w_i) - \sigma_2(1+w_i))}{g\,(1+w_i)}\, 10 \qquad (9.18)$$

The factor of 10 converts the units to g cm^{-2}. In practice the term (9.17) is approximated by 1.01325. w_i is taken to be 0.9 for water vapour and carbon dioxide.

The extinction coefficient also varies with temperature along an atmospheric path, and this is parametrised for carbon dioxide only (Slingo 1984) by scaling the path length in a layer (9.18) by a factor

$$\left(\frac{T}{263}\right)^{\max(8.5 + 2\log_{10}(\bar{\gamma}_i(\sigma_2,\sigma_1)),0)} \qquad (9.19)$$

A different approach is adopted for the water vapour continuum. Ignoring the small differences between definitions (9.6) and (9.7) we use the same function for the emissivity and absorptivity, namely (Slingo 1984):

$$\tilde{\epsilon}(p,p') = 1-e^{\left[-j_1 \frac{D}{g}\int_p^{p'} dp\, qp\, \{1 + \frac{j_2}{j_1}\frac{q}{0.622} e^{\left[\frac{1800}{T} - \frac{1800}{296}\right]}\}\right]} \qquad (9.20)$$

Here D is 1.66

q is the humidity mixing ratio

$\frac{j_1}{j_2}$ is fixed at 0.005

and j_i takes the value 0.05 in band 10

0.15 in band 9

0.35 in band 8

The code is organised so as to work upwards from the surface. At each level the source terms in equations (9.9), (9.10) and (9.15) are calculated and stored. A loop from the surface to the current level is then performed, calculating the terms linking two levels that appear in (9.9), (9.10) and (9.15) and these are added to the relevant fluxes. A schematic diagram of the longwave flux calculation is given in figure 9.6.

9.2 The flux of solar radiation

The total downward solar flux at height z will, in general, have two components - the direct, clear sky flux and the diffuse flux from the cloud: thus

$$S(z) = (1-Q)\, S^{\infty}(z) + Q\Lambda S^{C}(z) \qquad (9.21)$$

where Q is the cloud amount

Λ is the transmissivity of the cloud

$S^{\infty}(z)$ is the clear sky downward flux

$$S^{\infty}(z) = S\cos\xi \left[1 - \int_{o}^{\infty} d\omega\, A_{i\omega}(X\bar{y}(z,\infty))G(\omega) \right] \qquad (10.22)$$

and $S^{C}(z)$ is the downward flux coming from the cloud

$$S^{C}(z) = S\cos\xi \left[1 - \int_{o}^{\infty} d\omega\, G(\omega)A_{i\omega}(X\bar{y}(z_{ct},\infty) + 1.66\, \bar{y}(z,z_{ct})) \right] \qquad (9.23)$$

S is the solar consant, ξ is the zenith angle, $A_{i\omega}$ is the absorption of gas i at frequency ω, X is a magnification factor taking account of the greater amount of atmosphere traversed when the zenith angle increases, given by:

$$X = \frac{\left[1 + \frac{a}{z} \right]}{\sqrt{\left[\frac{2a}{z} + \cos^{2}\xi \right]}} \qquad (9.24)$$

where a is the radius of the earth, and $a/Z = 0.0078394$. Note that this reduces to sec ξ for small ξ

y is the pressure weighted path length given in (9.16), the factor 1.66 is an approximation due to Elsasser (Rodgers 1979) of the diffusion of the beam at cloud top and is the same 1.66 as occurs in (9.20), and $G(\omega)$ describes the frequency variation of the solar beam at the top of the atmosphere

$$S = \int_0^\infty d\omega (S_\omega(0)) = \int_0^\infty d\omega \; SG(\omega) \qquad (9.25)$$

The pressure weighting factor w_i, used to give the effective optical depth (9.16) for water vapour is again 0.9, but that for carbon dioxide varies from 0.4 to 0.9 (Hunt and Mattingly, 1974). In practice a linear interpolation is performed on the values for carbon dioxide path length used in the 11 layer atmospheric general circulation model.

The frequency integration is again performed by splitting the spectrum into bands. This time only two bands are required, one for carbon dioxide and one for water vapour. There is no significant overlap between the two, so the absorptions are simply added together. The water vapour absorption is shown as a function of optical depth in figure 9.7 and the carbon dioxide absorption in figure 9.8.

The reflected solar beam receives an extremely simple treatment, in that it is reflected straight to space, without absorption in its upward path. Cloud optical properties are listed in Table 9.1.

The albedo is specified according to the values given in Table B.3* unless the surface is sea, when $\alpha = 0.06$, snow-covered when $\alpha = 0.5$ or ice-covered when $\alpha = 0.8$. This albedo is changed to take account of multiple reflections between cloud and ground (see figure 9.9):

$$\alpha_{eff} = \frac{\alpha \left[1 - \{1 - \prod_{i=1}^{4} (1-Q_i)\} \quad \frac{\sum_{i=1}^{4} \beta_i S_i}{\sum_{i=1}^{4} S_i} \right]}{\left[1 - \alpha\{1 - \prod_{i=1}^{4} (1-Q_i)\} \quad \frac{\sum_{i=1}^{4} \beta_i S_i}{\sum_{i=1}^{4} S_i} \right]} \qquad (9.26)$$

where Q_i is the amount of cloud type i

β_i is the reflectivity of cloud type i

S_i is the solar flux reaching the earth's surface from cloud type i.

The solar constant is adjusted to take account of the eccentricity of the earth's orbit.

$$S = S_p (1 + e \cos\Omega_p)^2 \qquad (9.27)$$

* Dickinson and Temperton, Appendix B.

where S_p is the solar constant at perihelion, 1395 Wm^{-2}

e is the eccentricity of the earth's orbit, 0.0167

Ω_p is the angular distance from perihelion (January 3), assumed to vary linearly with time.

The solar constant is further reduced by a factor 0.97 as a crude approximation of Rayleigh scattering.

The code is organised so as to work downwards from the top of the atmosphere. The direct and diffuse path lengths are calculated and stored, and absorptions calculated from them. A schematic diagram of the shortwave flux calculation is given in figure 9.10.

As radiation increments cannot be calculated every timestep, the effects of solar radiation are meaned over the time between radiation calls by calculating a mean cosine of zenith angle:

$$\overline{\cos\xi} = \frac{\int_{h_1}^{h_2} [\cos\phi\cos\delta\cos(\lambda + \tau) - \sin\phi\sin\delta]d\tau}{h_2 - h_1} \qquad (9.28)$$

where ϕ, δ, λ, τ are as in (8.9)*, h_1, h_2 are the hour angles either for the time between radiation calls or for sunrise or sunset, whichever is appropriate.

* Dickinson and Temperton, Chp 8.

Since a little under half the points of a global model do not receive any solar radiation at any given timestep, the radiation code first sorts the gridpoints into those which receive solar radiation and those which do not. The code for the solar radiation calculation is then only called when appropriate.

9.3 The calculation of heating rates

We now have the upward and downward shortwave and longwave fluxes available at layer boundaries. The contributions from the different parts of the spectrum are added, and the downward flux subtracted from the upward flux to give the net flux. We now calculate the heating rate in a layer to be

$$\frac{\partial T_k}{\partial t} = -\frac{g}{c_p}\frac{\partial I_k}{\partial p} \approx -\frac{g}{c_p}\frac{(I_{k+1/2} - I_{k-1/2})}{p_*(\sigma_{k+1/2} - \sigma_{k-1/2})} \qquad (9.29)$$

and at the surface the heating rate is

$$\frac{\partial T_*}{\partial t} = \frac{I_*}{H} \qquad (9.30)$$

where I_k is the net flux at level k and

H is the thermal capacity of the soil, as in (8.5)*

* Dickinson and Temperton, Chp 8.

9.4 The Parametrization of Cloud

The cloud amounts Q used in (9.1), (9.13) and (9.21) are parametrized in a simple and computationally economical manner. Convective cloud amounts are calculated by scaling the convective mass flux against a theoretical maximum. The base and top of the convective tower are calculated within the convection scheme as described in section 6.6.*

Layer clouds are assumed to be one layer thick. In the absence of deep (≥5 layers) convection, layer clouds are free to occur in any layer: low clouds in layers 2 to 4, medium clouds in layers 5-9 and high clouds in layers 10-12. Cloud amounts are parametrized by a quadratic in relative humidity:

$$C_{H,M,L} = \begin{cases} \left[\frac{(h-h^c)}{(1-h^c)}\right]^2 & h>h^c \\ 0 & h\leq h^c \end{cases} \qquad (9.31)$$

where h is the relative humidity expressed as a ratio and h^c is a critical relative humidity, taken to be 0.85 in the operational model. The maximum value taken by (9.31) in the relevant layers dictates the cloud amount and that layer is the one occupied by the cloud.

If deep convection is predicted, then the cloud base is assumed to be at the base of the convective tower, and the quadratic (9.31) is evaluated at that level only. Only 10% of the convective cloud is assumed to occupy the full depth, the remainder being added to the layer cloud amount.

* Dickinson and Temperton, Chp 6.

A parametrization of marine stratocumulus (Slingo J. 1980) is also included in the low cloud amount. If there is no surface inversion a further term C_{sc} depending on inversion strength is added to (9.31)

$$C_{sc} = \begin{cases} -16.67 \frac{\partial\theta}{\partial p} - 1.167 & h>0.85,\ \frac{\partial\theta}{\partial p} \leqslant -0.07 \\ [-16.67 \frac{\partial\theta}{\partial p} - 1.167] \frac{(h-0.5)}{0.35} & 0.85 \geqslant h > 0.5,\ \frac{\partial\theta}{\partial p} \leqslant -0.07 \\ 0 & \text{otherwise} \end{cases} \qquad (9.32)$$

Cloud type	Reflectivity	Transmissivity	Absorptivity
High	0.2	0.75	0.05
Medium	0.6	0.3	0.1
Low	0.6	0.3	0.1
Convective	0.6	0.3	0.1

Table 9.1 Cloud optical properties

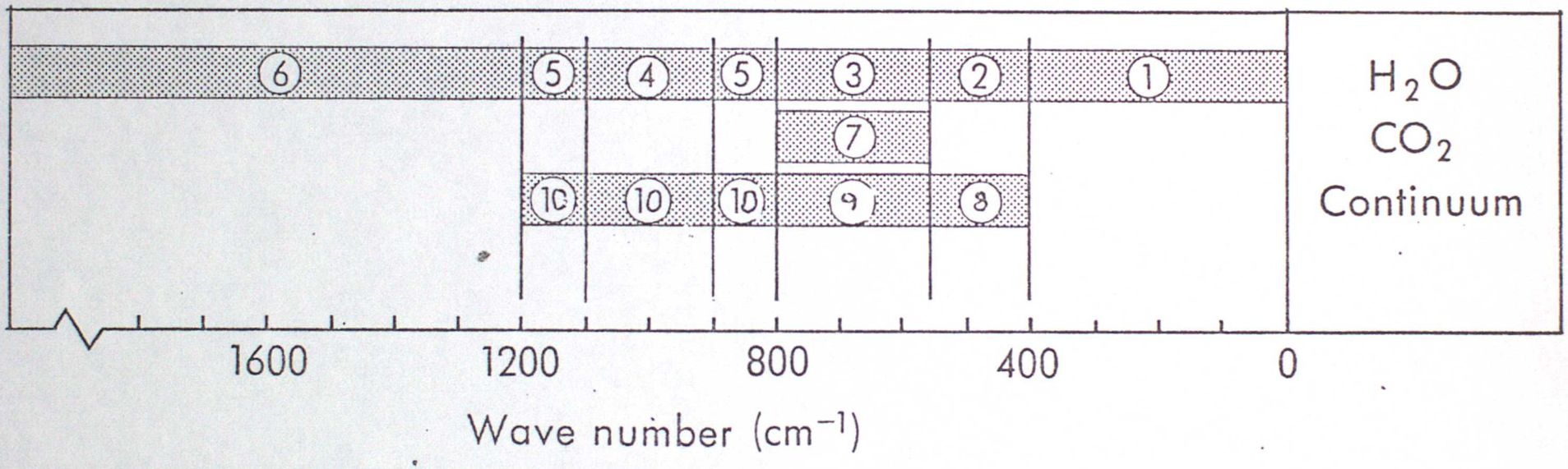

Figure 9.1 Spectrum bands used in the calculation of emmisivity and absorptivity.

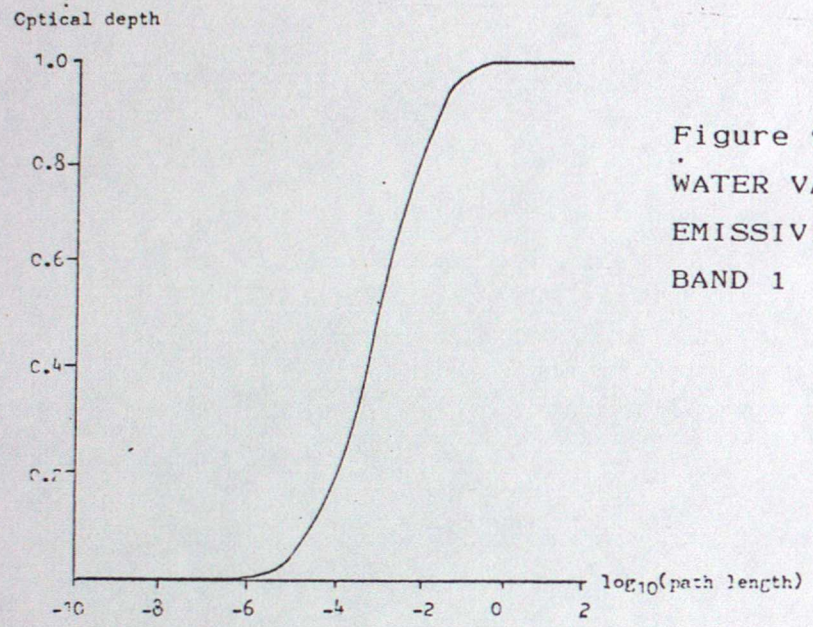

Figure 9.2a
WATER VAPOUR
EMISSIVITY
BAND 1

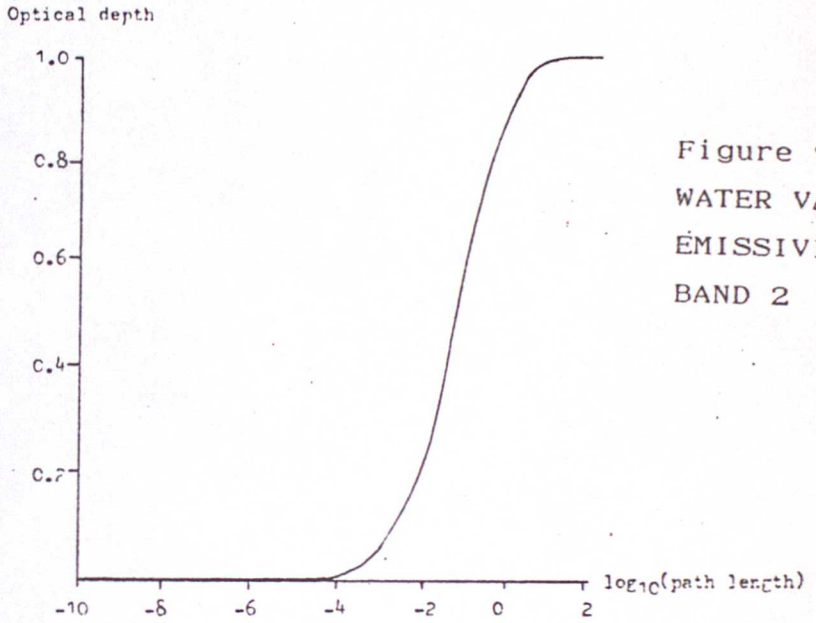

Figure 9.2b
WATER VAPOUR
EMISSIVITY
BAND 2

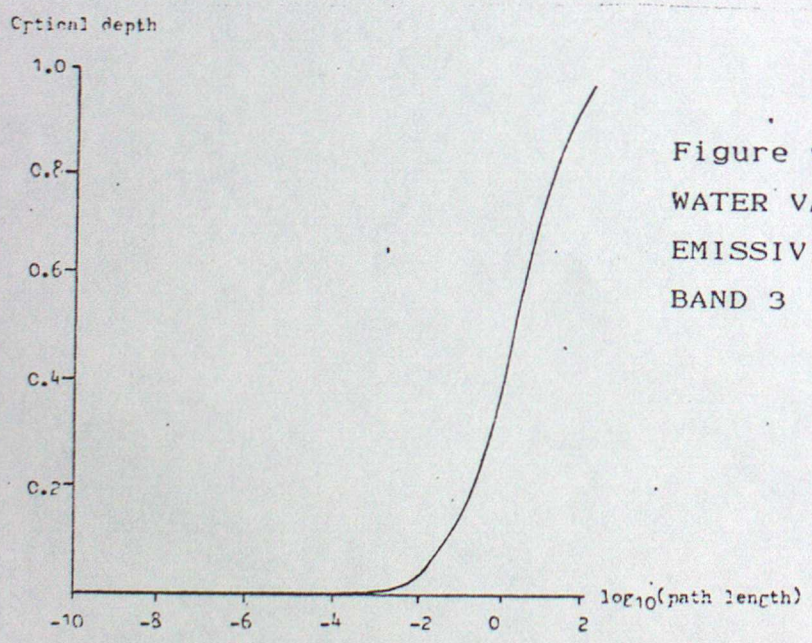

Figure 9.2c
WATER VAPOUR
EMISSIVITY
BAND 3

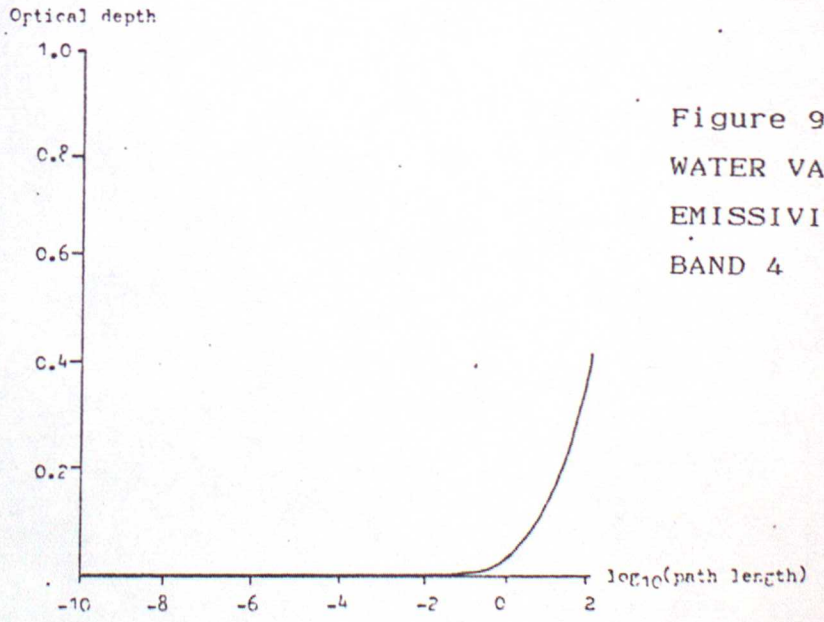

Figure 9.2d
WATER VAPOUR
EMISSIVITY
BAND 4

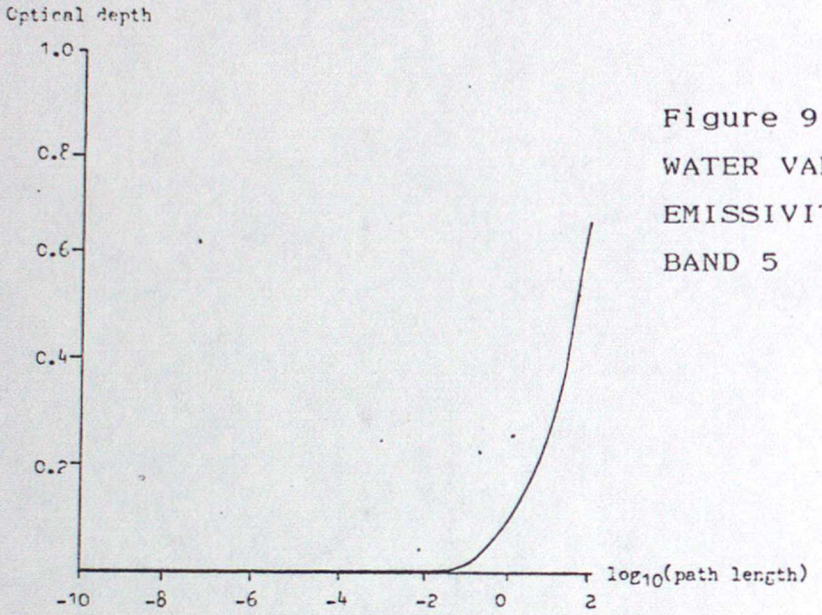

Figure 9.2e
WATER VAPOUR
EMISSIVITY
BAND 5

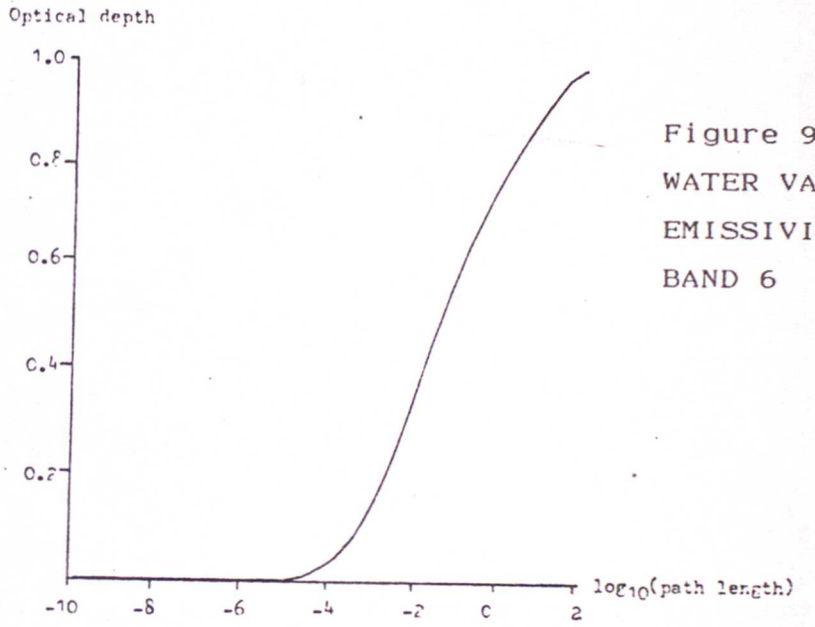

Figure 9.2f
WATER VAPOUR
EMISSIVITY
BAND 6

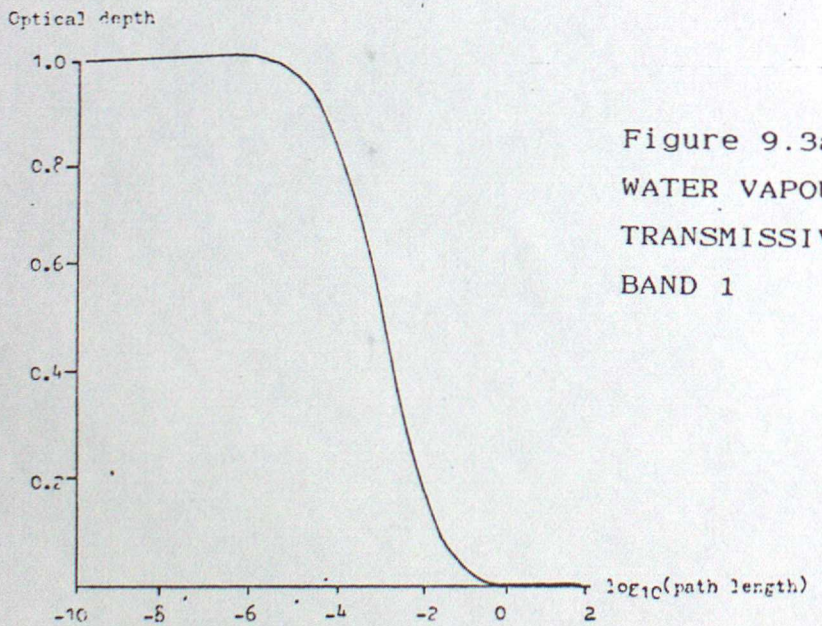

Figure 9.3a
WATER VAPOUR
TRANSMISSIVITY
BAND 1

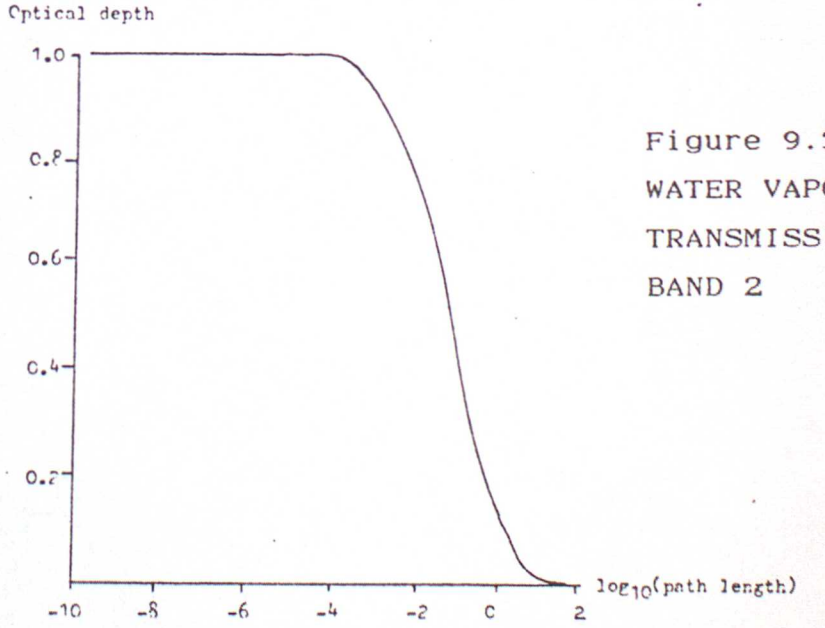

Figure 9.3b
WATER VAPOUR
TRANSMISSIVITY
BAND 2

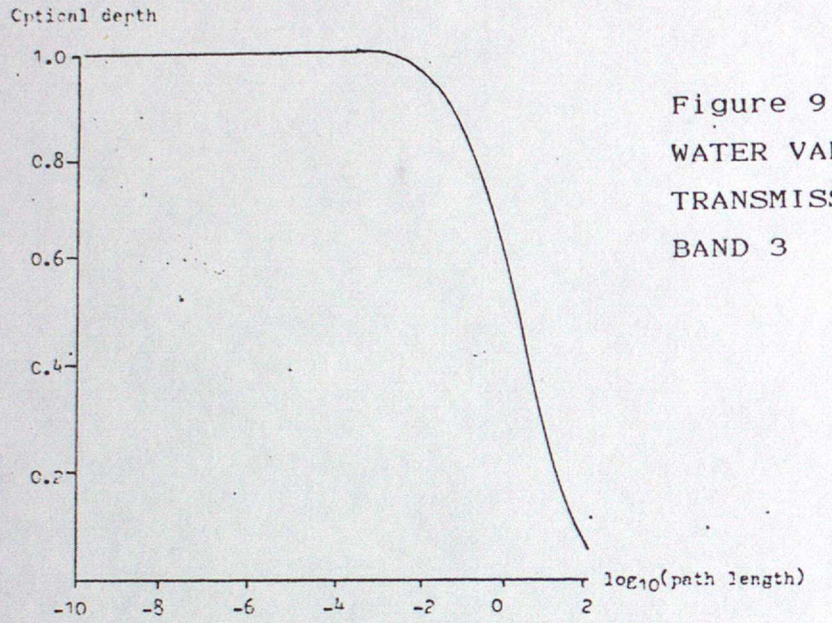

Figure 9.3c
WATER VAPOUR
TRANSMISSIVITY
BAND 3

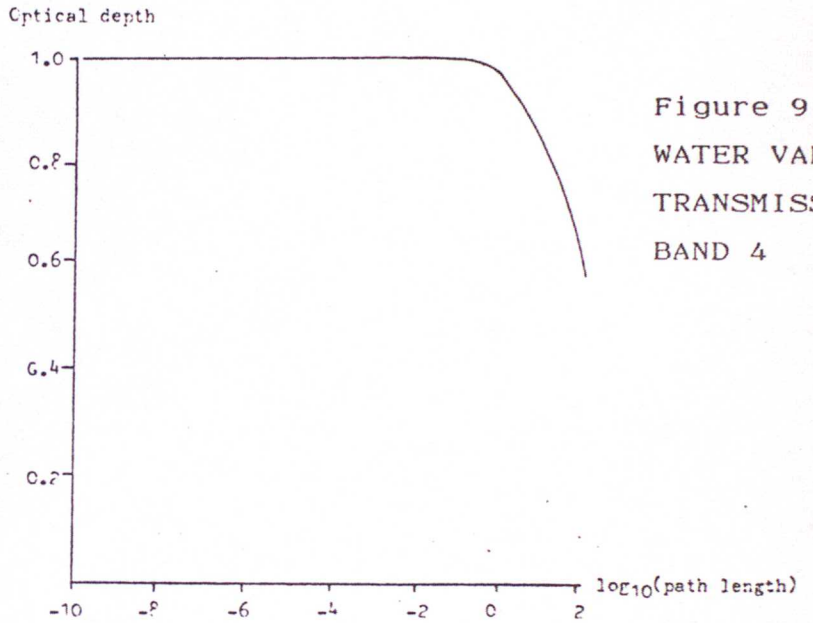

Figure 9.3d
WATER VAPOUR
TRANSMISSIVITY
BAND 4

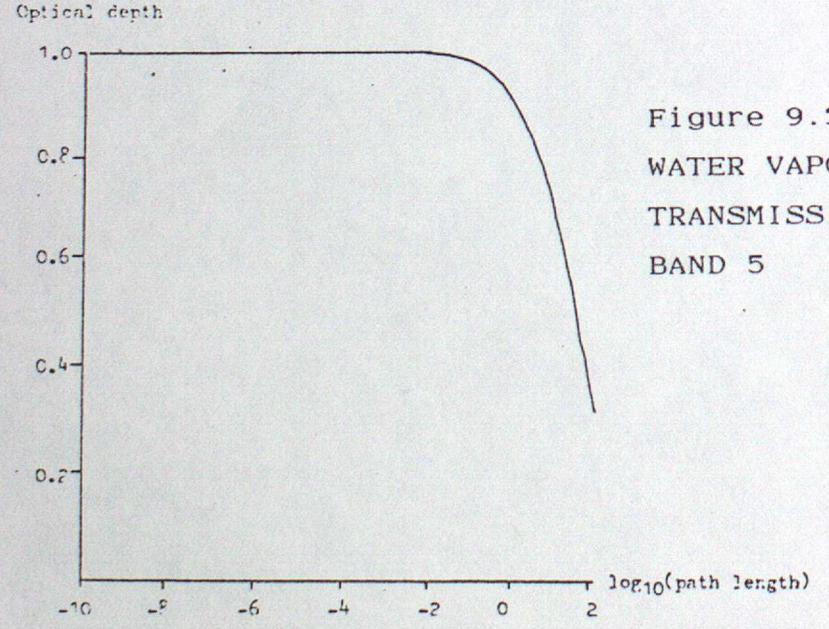

Figure 9.3e
WATER VAPOUR
TRANSMISSIVITY
BAND 5

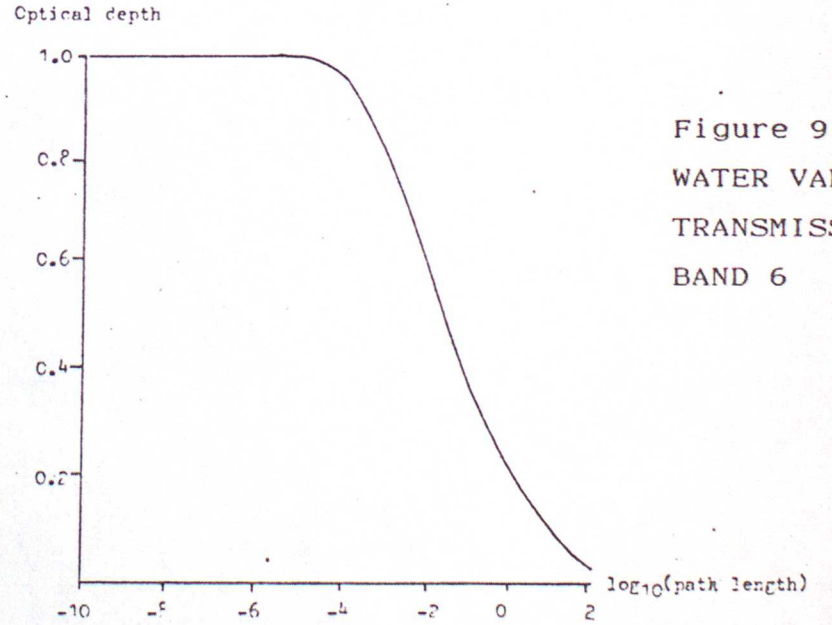

Figure 9.3f
WATER VAPOUR
TRANSMISSIVITY
BAND 6

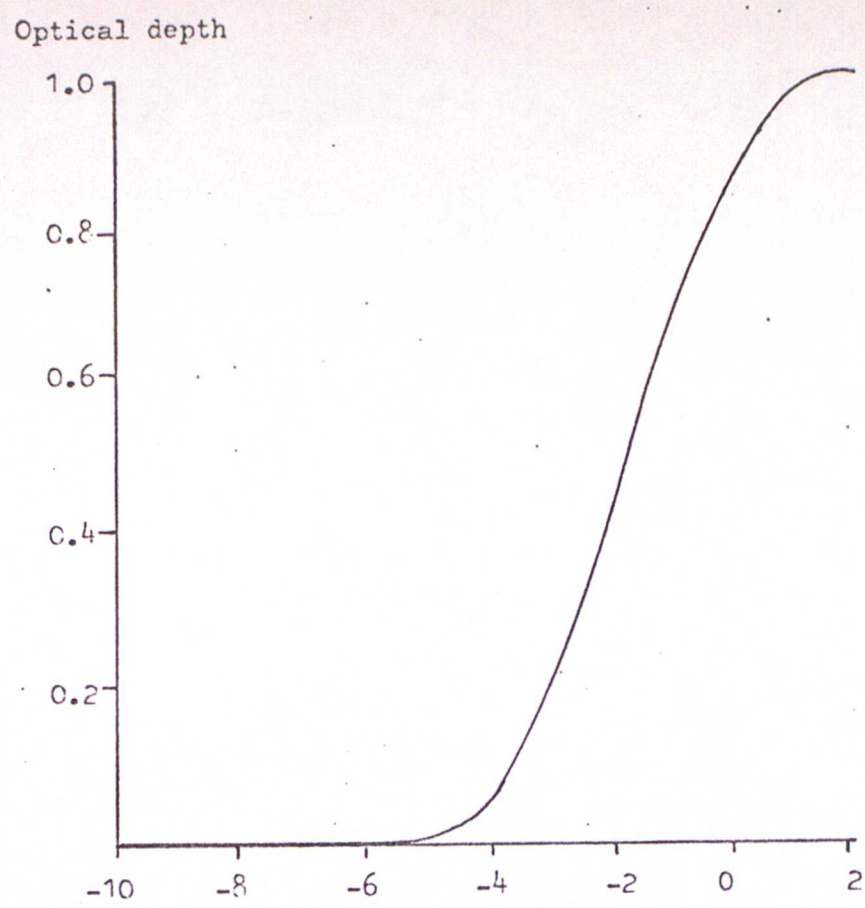

Figure 9.4
CARBON DIOXIDE EMISSIVITY

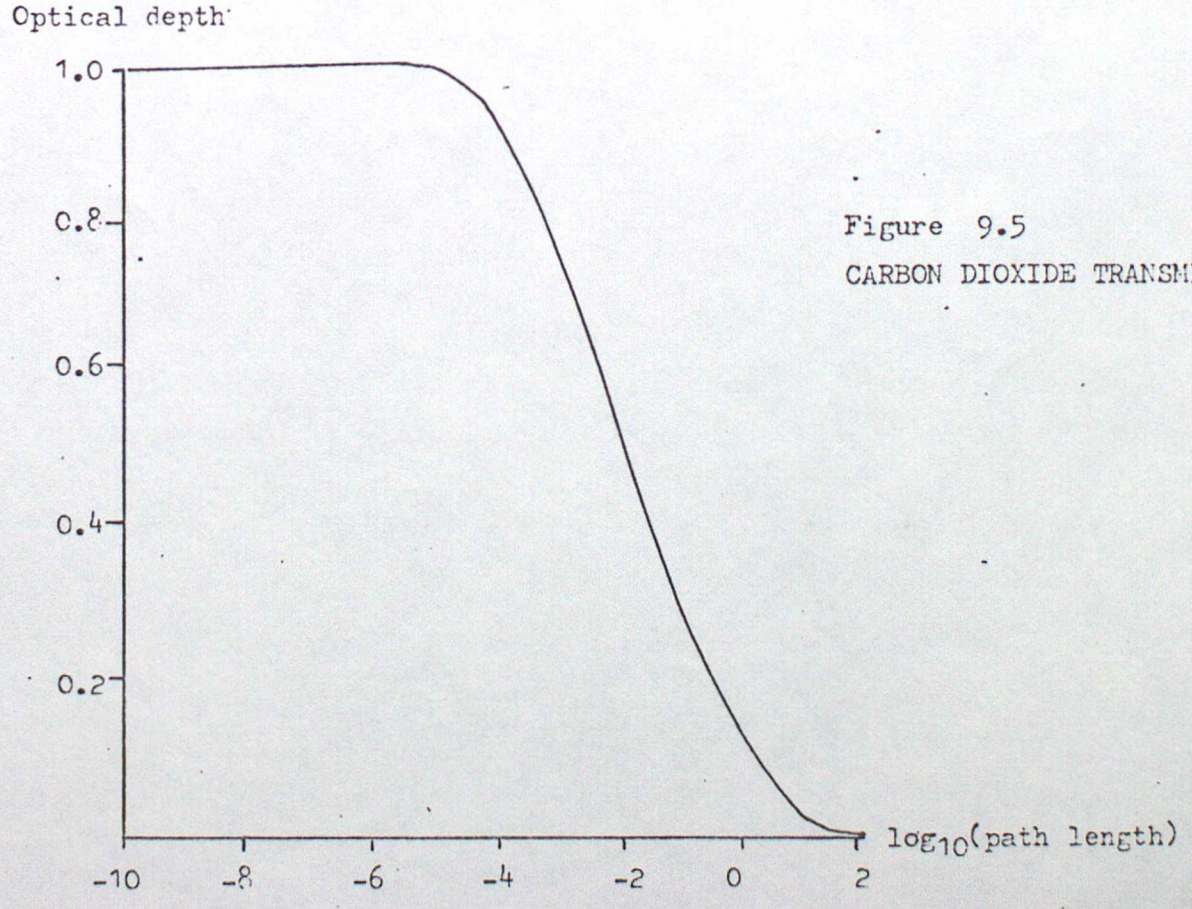

Figure 9.5
CARBON DIOXIDE TRANSMISSIVITY

Figure 9.6 Longwave fluxes at level z in a cloudy atmosphere.

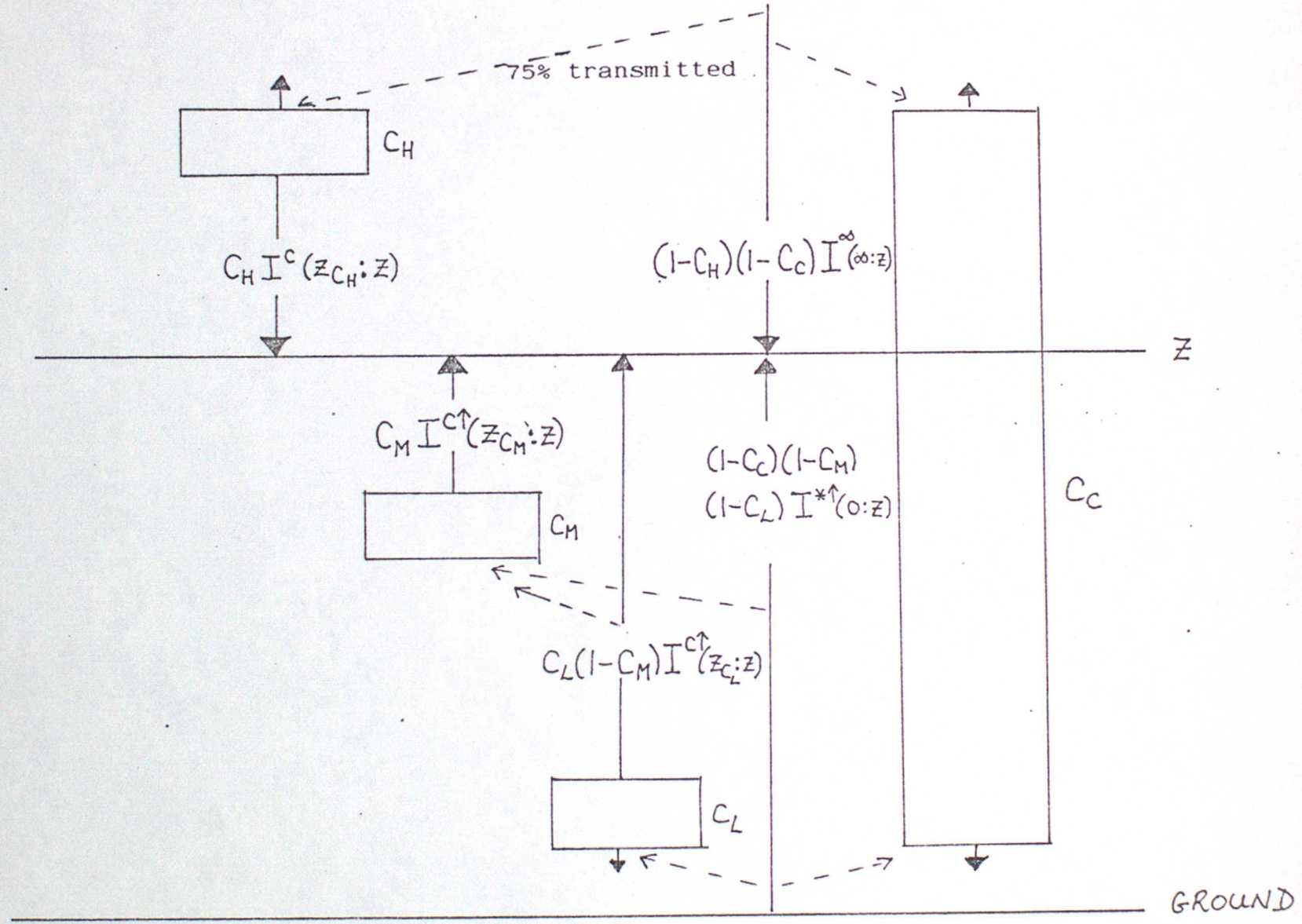

----> Unless otherwise stated these fluxes are assumed to be absorbed totally by the cloud.

Figure 9.7
WATER VAPOUR ABSORPTION

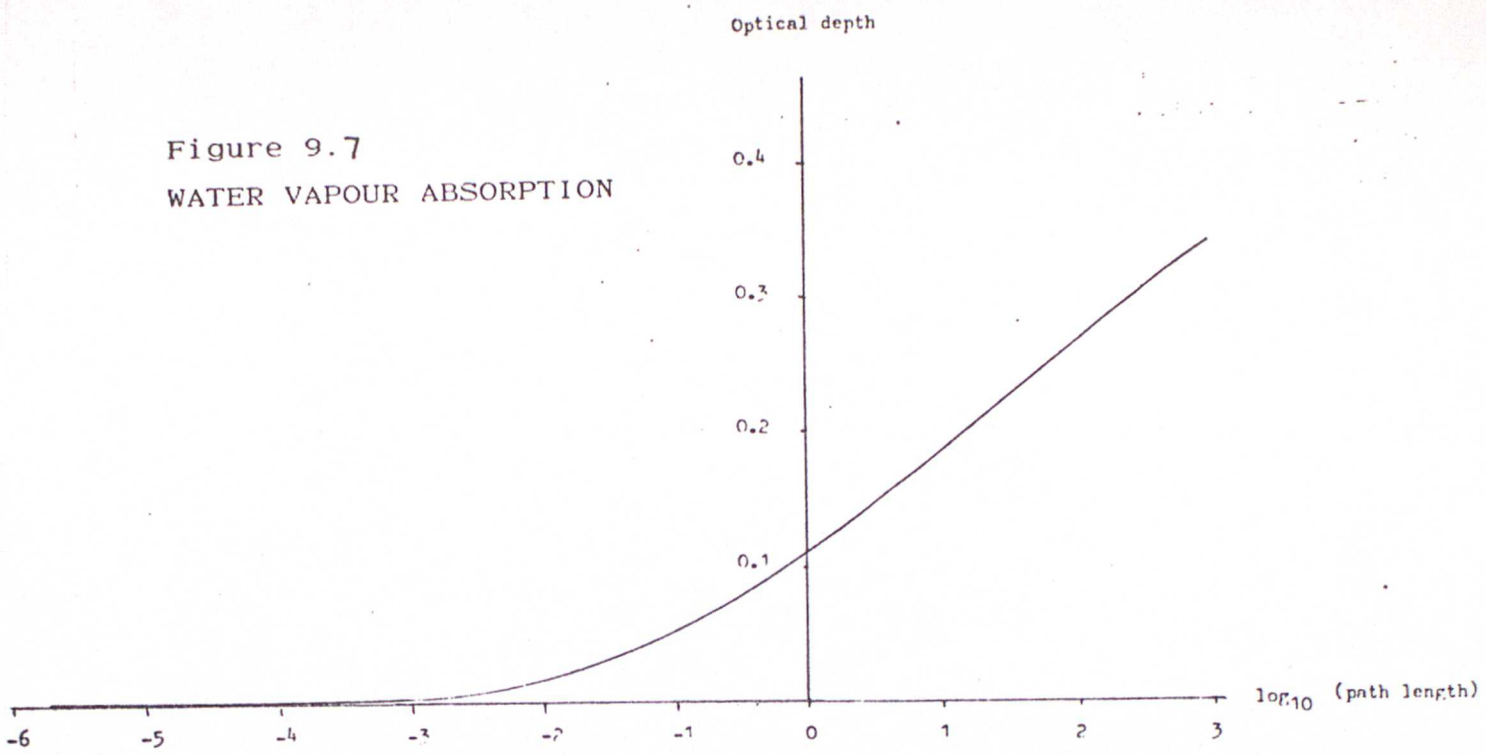

Figure 9.8
CARBON DIOXIDE ABSORPTION

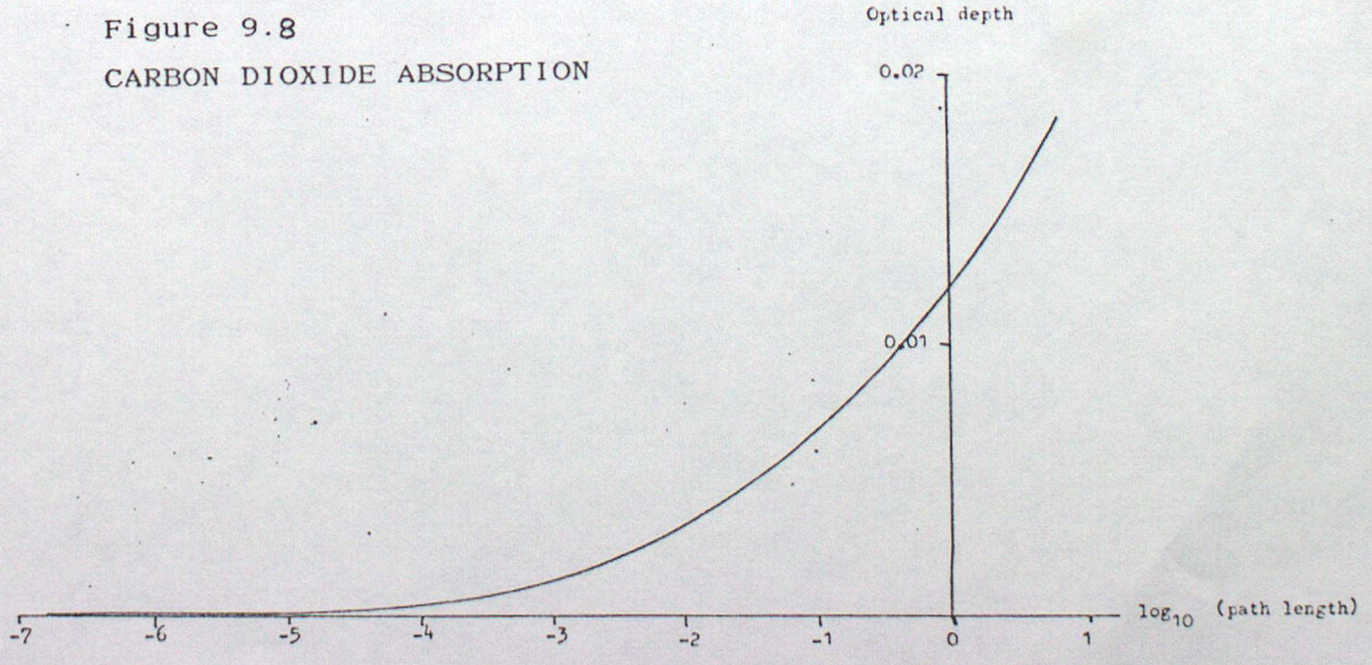

Figure 9.9 . Multiple reflections between clouds and the ground.

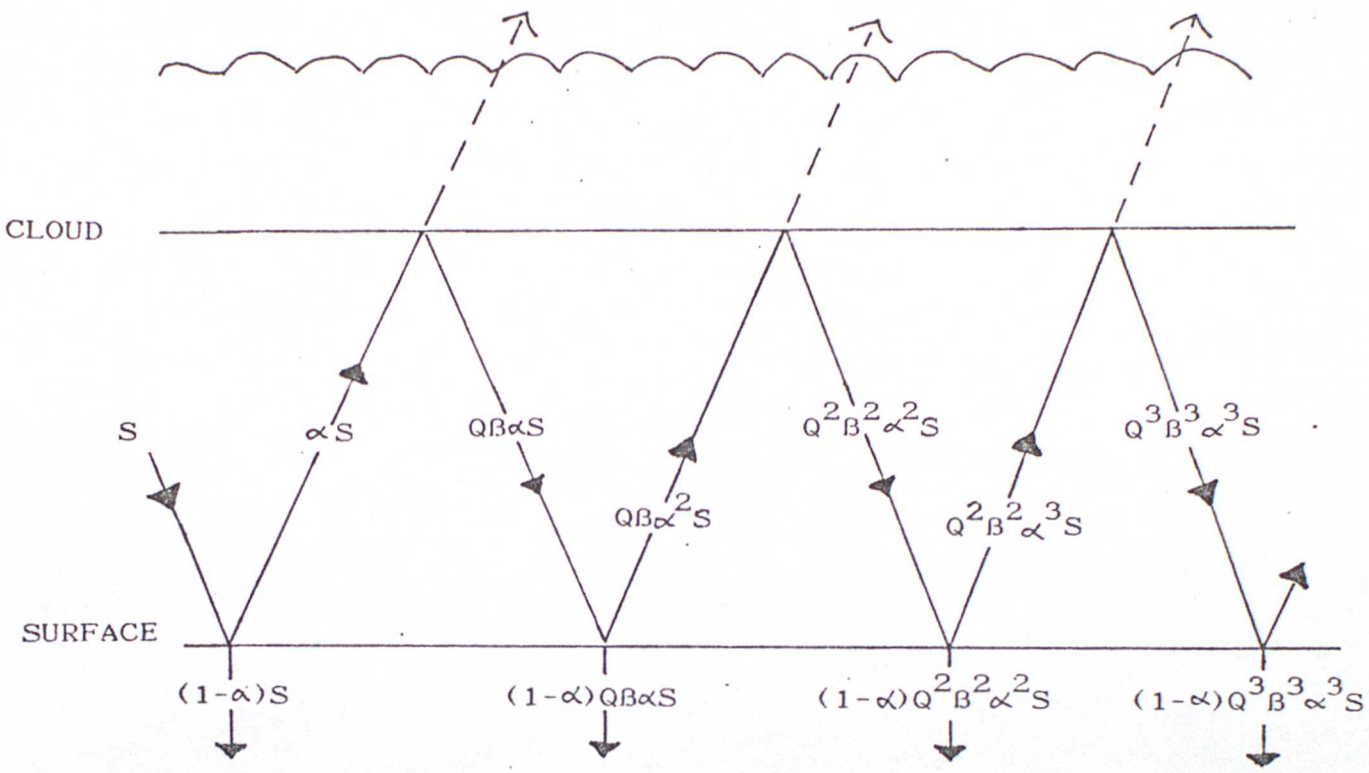

S = incoming solar flux

Q = cloud amount

β = cloud reflectivity

α = surface albedo

α_{eff} = effective surface albedo

Net solar flux absorbed by surface = $(1 - \alpha_{eff})S$

$= (1 - \alpha)S + (1 - \alpha)Q\beta\alpha S + (1 - \alpha)Q^2\beta^2\alpha^2 S$ .....

Therefore $(1 - \alpha_{eff}) = (1 - \alpha)(1 + Q\beta\alpha + Q^2\beta^2\alpha^2 + Q^3\beta^3\alpha^3$ .....)

$= (1 - \alpha)/(1 - Q\beta\alpha)$

Hence $\alpha_{eff} = (1 - Q\beta)/(1 - \alpha Q\beta)$

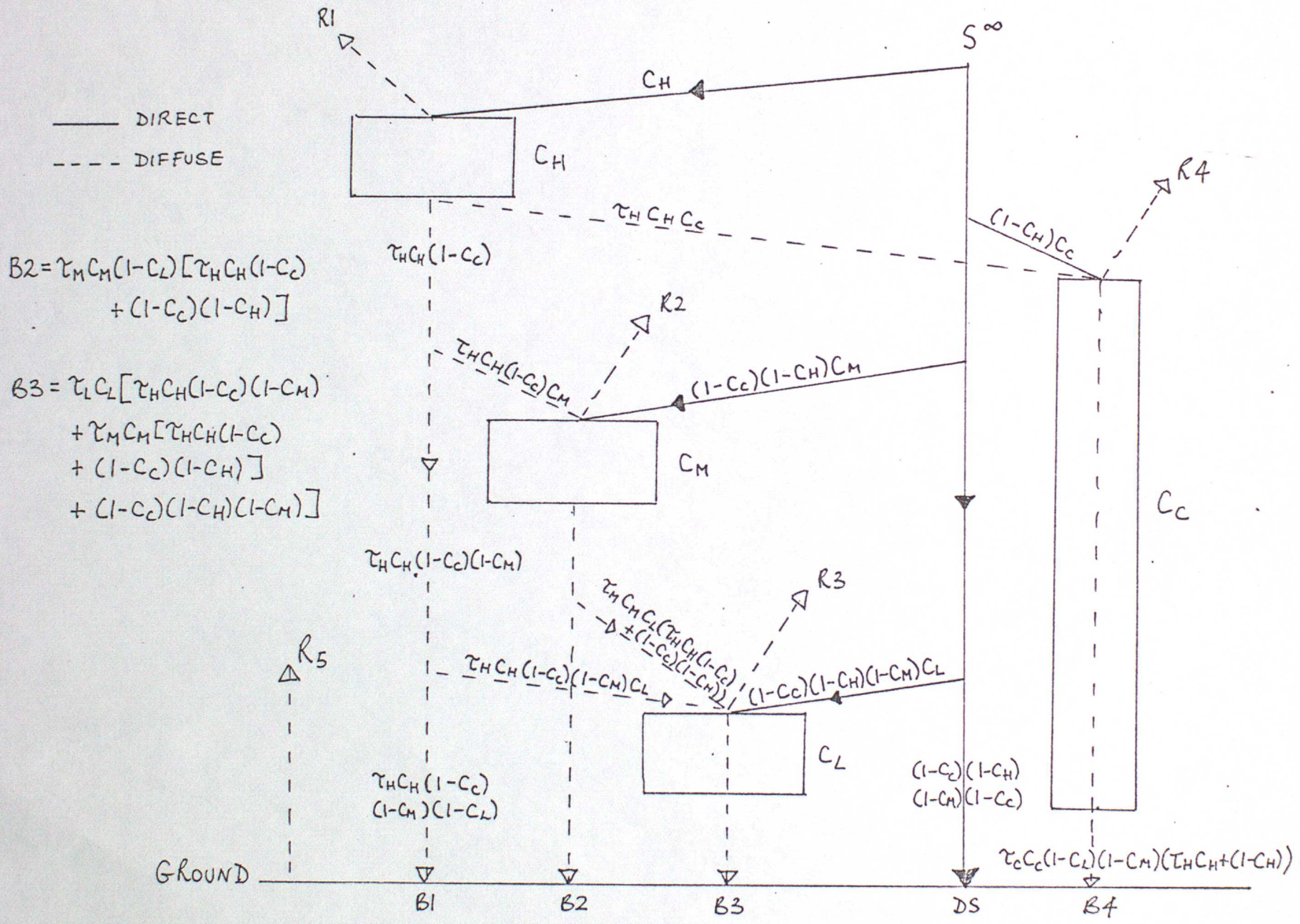

Figure 9.10 Division of the solar beam during its passage through a cloudy atmosphere.

References

Darlington, A	1985	An intercomparison of cloud prediction schemes. WGNE JSC study on radiation and clouds
Dickinson, A and Temperton, C.	1984	The operational numerical weather prediction model. Met O 11 Technical Note 183
Goody R M.	1964	Atmospheric radiation. Oxford University Press.
Hunt G.E. & S.R.Mattingly	1974	Atmospheric studies. Met O 20 Technical Note II/31
O'Neill A.	1974(a)	The eleven level radiation scheme: Part I Theory. Met O 20 Technical Note II/27
O'Neill A.	1974(b)	The eleven level radiation scheme: Part II Appendix to Part I. Met O 20 Technical Note II/28
Rodgers C.D.	1977	Radiation process in the atmosphere. ECMWF Seminars on the Parametization of the Physical Process in the Free Atmosphere, PP 5-66.
Rowntree P.R. and Julia Walker	1977	Radiation schemes in Met O 20 models. Met O 20 Technical Note II/93.
Slingo Julia M.	1979	A new interactive radiation scheme for the 5-level model. Met O 20 Technical note II/135
Slingo Julia M.	1980(a)	Interactive cloud and radiation in the Meteorological Office general circulation model, ECMWF Workshop on radiation and cloud-radiation interaction in numerical modelling 15-17 October 1980 pp 181-209
Slingo Julia M.	1980(b)	A cloud parametization scheme derived from GATE Data for use with a numerical model. Quart. J. R Met Soc 106 pp 747-770
Slingo A. and R.C.Wilderspin		Development of a revised longwave radiation scheme for an atmospheric general circulation model. Met O 20 DCTN 14
Walker Julia M.	1977	Interactive cloud and radiation in the 11-layer model Met O 20 Technical note II/91